CHAPTER IV

Microporous Membranes of Isotactic Poly(4-methyl-1-pentene) from a Melt-Extrusion Process: (II) Effects of Thermal Annealing and Stretching on Porosity

ABSTRACT

A two part study utilizing isotactic poly(4-methyl-1-pentene) (PMP) was undertaken to investigate a three stage process (melt-extrusion/annealing/uniaxial-stretching) (MEAUS) to produce microporous films. In this report, the thermal annealing (second stage) and subsequent uniaxial-stretching (third stage) results of selected PMP films from three resins, labeled A, B & C, are discussed. From sequential analysis of the effect each stage had on the resulting microporosity, it was discovered that the melt-extruded precursor morphology and orientation, as a consequence of the first stage extrusion parameters and resin characteristics, were crucial to controlling the membrane permeability. The annealing parameters were also critical, where a temperature of 205°C applied for 20 min. under no tension was the optimum annealing condition for producing highly microporous PMP films upon stretching. For the conditions studied, the stretching parameters that were found to be the optimum for producing the desired characteristics in the final film were a cold and hot stretch temperature of 70 and 180°C, respectively. The cold and hot stretch extension levels concluded to be the best were a cold stretch extension of 80 percent followed by hot stretching to 90 percent and thus a total overall extension level of 170 percent for the processing window studied. However, these results were only with respect to resin A films while resin B and C samples could not be produced into microporous films via the MEAUS process. In the case of the resin B films, their inability to be formed into microporous films was due to the presence of a higher level of comonomer in this resin, which adversely impacted the α_c relaxation. The resin C films were not formed into microporous films due to the relatively low crystalline orientation of the melt-extruded precursors from this resin.

4.1 INTRODUCTION

Polymeric microporous membranes are produced by a variety of methods with one of these is composed of three stages: melt-extrusion, thermal annealing, and uniaxial-stretching, which will be designated in this paper as the MEAUS method. Although there has been some published literature[1-3] and several patents[4-7], describing the MEAUS procedures for producing microporous membranes, a sequential study covering this method has never appeared in the published literature. This is true even though the underlying mechanisms and the means to attain the desired outcomes at each stage are generally known. For example, many of the references listed above describe the MEAUS process as being the deformation of a "hard-elastic" semicrystalline polymeric material. It is recognized in the literature that these materials emanate from semicrystalline materials possessing a parallel or planar stacked lamellar morphology. Additionally, this type of lamellar arrangement is a consequence of a row-nucleated morphology created by the appropriate melt-flow stress conditions in the course of extrusion.

In the first paper[8] of this two part investigation, the melt extrusion results of three poly(4-methyl-1-pentene) (PMP) resins (A, B & C) were discussed. The resins differed mainly in weight average molecular weight (M_w), although resin B had approximately double (6.5 wt%) the level of a 1-olefin comonomer (1-decene from solution NMR measurements) possessed by resins A or C. Upon melt extrusion, precursor films possessing stacked lamellar morphologies were obtained from each resin. In the case of resin A, the films all possessed parallel planar lamellae textures for the process window studied. However, only select films from the other two resins (B & C) were characterized by planar lamellar structures. The chain axis crystal orientation with respect to the machine direction (MD) was also determined for these precursors utilizing wide-angle X-ray scattering (WAXS). When the precursors were melt-extruded under similar conditions, it was found that resin A films possessed the highest chain axis orientation followed by the resin B films and lastly the resin C films. These morphological and orientation results were concluded to be a consequence of the process conditions and melt-relaxation times, where the highest M_w resin (A) possessed the longest melt-relaxation time, followed by the intermediate M_w resin (B), and the lowest M_w resin (C).

To generate microporosity in these melt-extruded precursor films, an annealing stage is also required.[9] Its utility is believed to be in the promotion of small-scale structural modifications in both the crystalline and amorphous phases, accomplished in the MEAUS process through control of the annealing temperature (T_a), time (t_a), and tension level (percent extension) applied to the film during this stage. The desired modifications in the crystalline regions are thickening and

perfection of the lamellae promoted at annealing temperatures below the melting point (T_m) but above the glass transition temperature (T_g). In the amorphous regions, the interlamellar linkages (tie-chains) are also thought to become less taut and in some cases are believed to be "reeled-in" thus potentially leading to fewer tie-chains.[10] The effects just described are possible for a semicrystalline polymer, *only if it possesses an α_c relaxation*,[10-12,] and in addition, according to Rault,[10] only if it is annealed at a temperature above the maximum value of the α_c relaxation ($T_{\alpha c}$).

The α_c relaxation is associated with chain axis translational mobility of the non-chemical defects in the crystal lattice. Since polymeric relaxations are not only temperature dependent but also frequency dependent, this particular value ($T_{\alpha c}$) is somewhat arbitrary but can be determined via dynamic mechanical spectroscopy (DMS) for a given frequency. The existence of such a relaxation is "necessary, but not sufficient"[14] for lamellae to thicken because the presence of noncrystallizable units along the polymer backbone (comonomer, branches, etc.), highly entangled interlamellar regions, and the nature of the morphology may effect the crystalline thickening process.[14] Boyd suggests, the α_c relaxation is only a characteristic of polymers that can not be rapidly cooled into a completely amorphous material. He categorized such polymers as "high" crystalline materials.[12,13] Linear high density polyethylene (HDPE) fits this classification based upon its relatively fast crystallization rate and reported α_c relaxation(s).[11,12,15-17] Both isotactic polypropylene (iPP)[10,16] and isotactic PMP[10] are also known to each possess an α_c relaxation. In fact, microporous membranes are commercially available from HDPE and iPP produced via the MEAUS process that is under discussion.[18]

The ability of the chains to translate through the crystalline lamellae also enables polymers possessing the α_c relaxation to be drawn or deformed to higher levels than those that do not possess this relaxation. In fact, it has been recognized that ultradrawing and solid-state processing of semicrystalline polymers possessing an α_c relaxation are possible, and the polymers that do not have this crystalline mobility are unable to undergo either ultradrawing or solid-state processing.[19-21] Ultradrawing is defined as achieving draw ratios (L/L_o) greater than 20 where L is the final sample length and L_o is the initial sample length. Higher extensibility also permits greater levels of lamellar separation (splaying) and subsequent local drawing in some cases upon stretching, the third stage of the MEAUS process. This third stage is composed of two stretching steps followed by a thermal-relaxation/heat-setting step. The first step is designated the "cold" stretch while the second is the "hot" stretch. The cold stretch temperature (T_{cs}) generally occurs above the polymer T_g but below the hot stretch temperature (T_{hs}), which

itself is below the annealing temperature of the prior stage but still in the upper temperature range of the α_c relaxation for a given polymer. The extension levels utilized during the cold stretch (%CS) and hot stretch (%HS) steps also need to be considered. The stretching directions in both steps are along the MD of the annealed film, i.e., perpendicular to the stacked lamellae. Cold stretching is utilized to "nucleate" the micropores via a ductile drawing of the amorphous and crystalline phases. The hot stretch step further splays the lamellae (i.e. increases the pore size) via a partial ductile drawing of the crystal phase. Following the stretching steps, the thermal-relaxation/heat-setting step is employed to allow partial recovery of the film in the first case while the latter is to impart dimensional stability after removal from the stretching oven and stretching apparatus. As has been observed in a previous dissertation study[3] using melt-extruded HDPE films[2], the uniformity and number of these microvoids can be influenced through the processing conditions at each stage (melt-extrusion, annealing, and stretching). Since control of the micropore structure and the film permeability is highly desirable, it is essential to understand the variables that can alter the quality of the microporosity produced upon annealing and subsequently stretching the melt-extruded films.

As stated above, this report is the second in the series that presents findings from the sequential study of the MEAUS process utilizing PMP. It is the main goal of the overall study that the information obtained will lead to a better understanding of how to control the microporous behavior of the final stretched PMP membranes. This will be accomplished by the sequential analysis of the results from each of the three process stages. The results of the first stage (melt-extrusion) have already been presented and discussed[8] with limited reiteration above. In this second paper, the annealing (second stage) and stretching (third stage) results are presented for selected melt-extruded PMP films from that earlier work. Furthermore, the same sample designation will be utilized for continuity. Specifically, in this report, we will address samples, A1, A2, B1, and C1, that were extruded under the conditions stated in Tables 2-4 from reference 8. These melt-extruded precursor films were chosen based upon their morphological features and orientation state in order to investigate the effects of specific annealing (T_a, t_a & tension) and stretching process variables (T_{cs}, %CS, T_{hs} & %HS). In our first report[8], the authors suggested some prerequisites for the production of a membrane with a high concentration of micropores uniformly distributed throughout the film. Two of the prerequisites were that the precursor should possess a parallel planar stacked lamellar morphology and a relatively high crystalline orientation. In fact, films A1, A2, and B1 each possessed these precursor characteristics while sample C1 had a lower crystalline orientation, as will be reviewed shortly.

Thus, the precursor films based on resin A (A1 & A2) will be the particular focus of this report, and samples B1 and C1 will be analyzed to a lesser extent.

4.2 EXPERIMENTAL

Materials

Melt-extruded precursors were selected from each of the three PMP resins A, B, and C. Besides obvious molecular weight differences, listed in Table 4.1, and as stated earlier, resins A and C are believed to possess approximately the same amount of 1-decene, ca. 3.2 wt %. Additionally, resin B was determined to have nearly double this amount, as measured via solution NMR.[22] The additional comonomer content of resin B will be shown later to influence the α_c relaxation of resin B precursors.

Table 4.1 Molecular weight characteristics for the three PMP resins studied

Sample	M_n (kg/mol)	M_w (kg/mol)	M_w / M_n
Resin A	44.5	460	10.3
Resin B	58.0	360	6.2
Resin C	36.9	290	7.8

Structural and Optical Techniques Utilized

Wide-Angle X-ray Scattering (WAXS)

WAXS studies were performed on a Philips table-top x-ray generator model PW1720 equipped with a standard vacuum sealed Warhus photographic pinhole camera. The X-ray beam was of Cu Kα radiation, λ = 1.544 Å, and was collimated to a beam diameter of 0.020 inches (0.508 mm).

Since the extrusion lead to planar extensional flow along the MD, this promoted uniaxial orientation behavior with respect to the MD axis.[2] As a result, the nature of the crystalline orientation distribution (orientation function) need only be obtained by examination of the azimuthal angle dependence of different reflections arising from standard flat plate WAXS patterns. The orientation function utilized was the Hermans' orientation function (f_H),[23]

$$f_H = \frac{(3 \cdot \overline{\cos^2 \theta} - 1)}{2} \qquad \text{(Eqn. 4.1)}$$

where θ is the angle between the chain or specific unit cell axis and a chosen reference axis, which is the MD in our case. The procedural details for determining the crystalline orientation (f_c) in the PMP films discussed in this paper has been given in our first report[8].

Infrared Linear Dichroism

A Nicolet 510 FTIR. spectrometer equipped with a wire grid polarizer was used for determining FTIR dichroism, which is defined as

$$D = \frac{A_{II}}{A_{\perp}} \qquad \text{(Eqn. 4.2)}$$

where A_{II} is the absorption parallel and $A_{\perp}$ is the absorption perpendicular to a specific reference axis. For uniaxial orientation, the dichroic ratio is related to the Hermans' orientation function by the following relationship

$$f_H = \left[\frac{(D_o + 2)}{(D_o - 1)}\right]\left[\frac{(D - 1)}{(D + 2)}\right] \qquad \text{(Eqn. 4.3)}$$

where $D_o = 2\cot^2\alpha$, and the value for α is the angle between the chromophore transition moment and the chain axis. For PMP, a vibration specific to a single phase is not known. He and Porter[24], however, have used the dichroism of the 918 cm^{-1} band, a rocking mode vibration from two methyl groups[25], to follow sample orientation as a function of extension. We have also utilized this absorption band in this study.

Atomic Force Microscopy (AFM)

AFM micrographs were obtained with the use of a Digital Instruments Nanoscope III Scanning Probe Microscope operated in TappingMode™. Nanosensor TESP single beam cantilever tips possessing force constants of 35±7 N/m and oscillated at frequencies of ca. 290 kHz were used. The films were placed upon glass slides using double stick tape with raster-scanning of the sample done parallel to the machine direction of the film.

Transmission Electron Microscopy (TEM) and Scanning Electron Microscopy (SEM)

Transmission electron microscopy micrographs were taken with a Philips EM-420 scanning transmission electron microscope (STEM) utilizing the procedures presented in the initial report for this study[8].

Differential Scanning Calorimetry (DSC)

DSC measurement was performed with a Perkin-Elmer DSC-7. Heating scans were conducted utilizing the procedures presented in our initial report[8].

Dynamic Mechanical Spectroscopy (DMS)

Dynamic mechanical testing was carried out on a Seiko instruments DMS 210. The samples were tested in tensile mode using samples approximately 0.0254 mm thick, 10 mm long, 6 mm wide. The DMS experiments were performed at a frequency of 1 Hz using a heating rate of 2°C/min under N_2 atmosphere.

Gurley Instrument and Film thickness

Film porosity was determined by measuring the stretched film permeability given in terms of a parameter called Gurley number. The Gurley number is defined as the time required for 10cc of air to pass through a 1 inch square section of film at a constant pressure of 12.2 inches of H_2O where the Gurley number is given in units of seconds. It is thus an inverse index of permeability where a *greater Gurley number implies a lower permeability*.[3] The Gurley number measurements were performed using a Gurley densometer model no. 4150. In this report, a "quality" microporous film is defined as a film possessing Gurley number less than 100 sec. A *minimum* of six Gurley measurements were made for each stretched film. Film thickness measurements were carried out on a Series 400 Precision Micrometer.

4.3 RESULTS

As previously stated, four extruded films, A1, A2, B1, and C1, were utilized for this study, and all four films possessed stacked lamellar morphologies that were in some cases planar. Table 4.2 provides this information along with other pertinent film characteristics. Because of the large number of annealing and stretching variable combinations utilized, only selected annealing and stretching results will be presented that are, in general, representative of most of the PMP films studied.

Table 4.2 Pertinent characteristics of the precursor films utilized in this study.

Sample	Lamellar Morphology	f_c	X_c (%)	T_m (°C)
A1	Planar	0.89	63	229
A2	Partially Twisted	0.83	62	231
B1	Planar	0.84	42	221
C1	Partially Twisted	0.67	63	231

4.3-1 Annealing (Stage Two):

The annealing temperatures studied were selected based upon the range of temperatures encompassing the PMP mechanical α_c relaxation, as expressed by Tan δ, for the resin A or C precursors are shown in Fig. 4.1. It is observed that the range of temperatures encompassing the α_c relaxation for either the resin A or C film is approximately 60-235 °C with the maximum ($T_{\alpha c}$) occurring at ca. 140°C. In fact, the α_c relaxations of these two films are similar in shape (not magnitude). In contrast, film B1 possesses an α_c relaxation that is partially convoluted with the T_g and is likely a consequence of the crystalline imperfection due to the additional comonomer present in resin B. From this analysis of the PMP films, annealing temperatures equal to 145, 160, 180, and 205°C, were selected. The upper annealing temperatures were also slightly below and above the approximate onset of the PMP melting endotherm – see Fig. 4.2.

The annealing times employed were 5, 10, and 20 min. These were chosen in light of feasible industrial processing times. The tension level was divided into two main categories: annealing without tension (free-anneal or 0% tension) and annealing under a specified level of tension where in the case of the latter, the levels of tension (extension) were 3, 9, and 15 percent. These levels were applied during the annealing stage with a small mechanical stretching device. This device was the same one employed in the stretching stage. The effect of tension during annealing is important to the industrial scale process, where a certain amount of film extension (tension) is applied to keep the film taut while it proceeds through the annealing oven in a continuous process. The level of tension may alter the film morphology and crystalline orientation prior to stretching, which in turn can effect the microporosity and the morphology of the microporous film. The specific levels of tension utilized for the present study are, in part, based upon the previous work of Yu on HDPE films[3], where tension was observed to affect the annealed film morphology and crystal orientation (f_c), as discussed later.

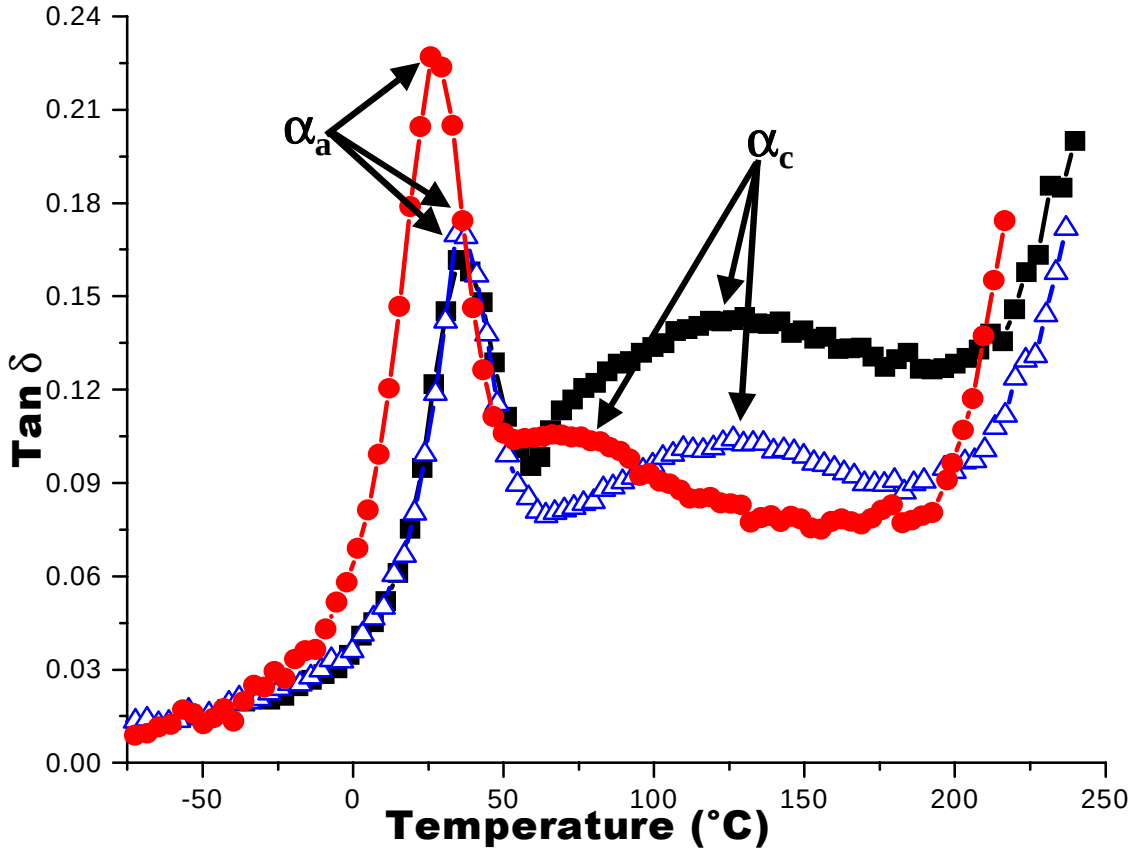

Figure 4.1 Tan δ as a function of temperature for PMP films (-■-) A1, (-●-) B1, and (-△-) C1 with their corresponding α_a (T_g) and α_c relaxations labeled. This data was obtained utilizing a heating rate of 2°C/min and a frequency of 1.0 Hz.

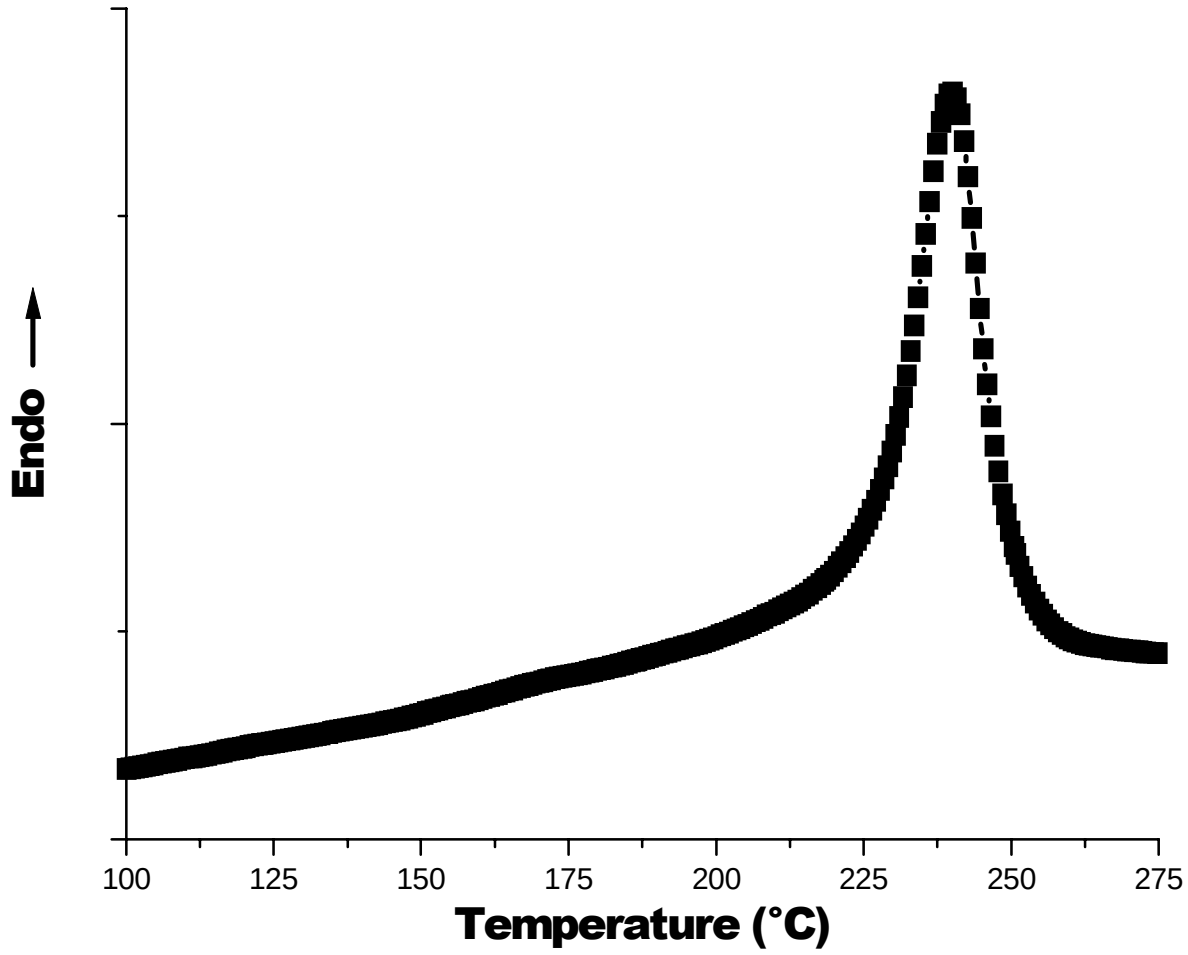

Figure 4.2 DSC heating scan of PMP resin A where a heating rate of 30°C/min was employed.

In Figs. 4.3a-d, the WAXS diffraction patterns are displayed for four A1 films: the precursor (i.e., non-annealed), a free-annealed film, a film annealed under 3 percent tension, and a film annealed under 15 percent extension, respectively. The annealed films presented in this figure utilized an annealing temperature equal to 205°C for a time of 20 min. It is observed that the azimuthal dependence of the (200) reflection, indicated by arrows in Fig. 4.3a, is relatively high for all three films. This reflection was utilized here to calculate f_a and thus f_c. It was found that the main chain crystal orientation increases with the application of tension during annealing, other variables being equal. Figure 4.4 displays the f_c results for the A1 annealed films as a function of tension level and annealing temperature for a fixed annealing time of 20 minutes. Although the measured change in f_c is small, it does systematically increase as the specific tension level is increased for a fixed annealing temperature. Additionally, the crystalline orientation becomes greater along MD as the annealing temperature is raised for a fixed extension level, as long as the tension level is greater than zero.

The effect of annealing time in conjunction with tension level on f_c is displayed in Fig. 4.5 for the fixed annealing temperature of 205°C. It is recognized that with increasing annealing time and increasing tension that f_c increases asymptotically, although the overall change in f_c is small. The trends in these results were qualitatively supported with IR dichroism measurements, as displayed in Fig. 4.6, which is a plot of the dichroic ratio (D) for the 918 cm^{-1} band and is expressed as a function of annealing time and level of tension. As extension level increases, the dichroic ratio, which in this case is related to the overall sample orientation, asymptotically increases for a fixed annealing temperature (205°C) and a fixed annealing time. Further, as the annealing time increases from 5 to 20 minutes, the dichroic ratio increases as did f_c, as obtained by the WAXS results presented previously in Fig. 4.5. An example of the parallel and perpendicular FTIR absorption spectra for the PMP films is shown in Fig. 4.7, which is of the A1 precursor. A fact not yet addressed that arises from Figs. 4.3-4.6 is that for the *free-annealed* specimens, the crystalline orientation is *not affected* by annealing time or temperature. In summary, the orientation results presented in Figs. 4.3-4.6, were representative for all the films prepared from all resins.

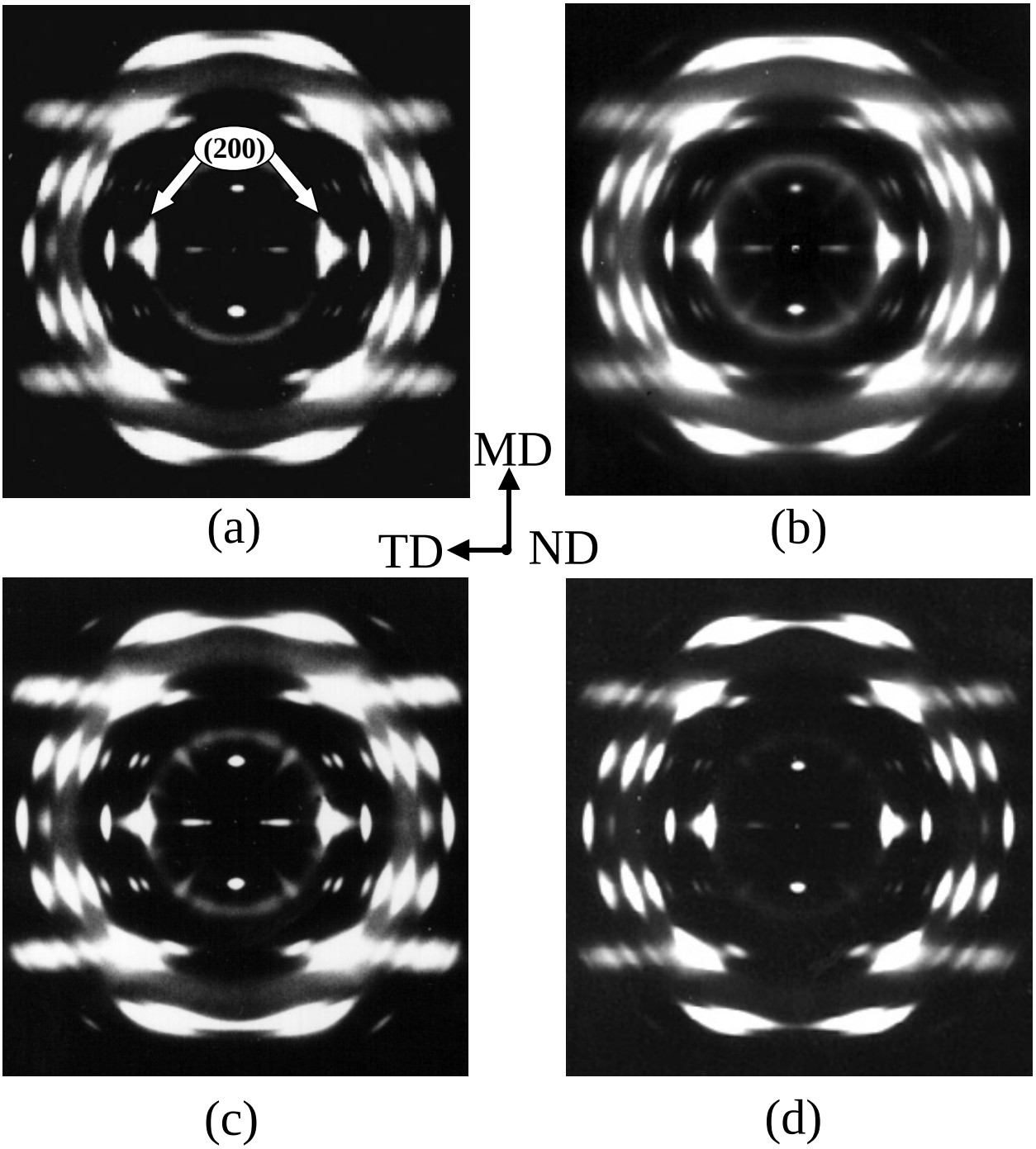

Figure 4.3 WAXS photographs of A1 films a) precursor, b) free-annealed at T_a = 205°C for t_a = 20min, c) 3 % tension T_a = 205°C for t_a = 20min, d) 15% tension T_a = 205°C for t_a = 20min. MD direction shown.

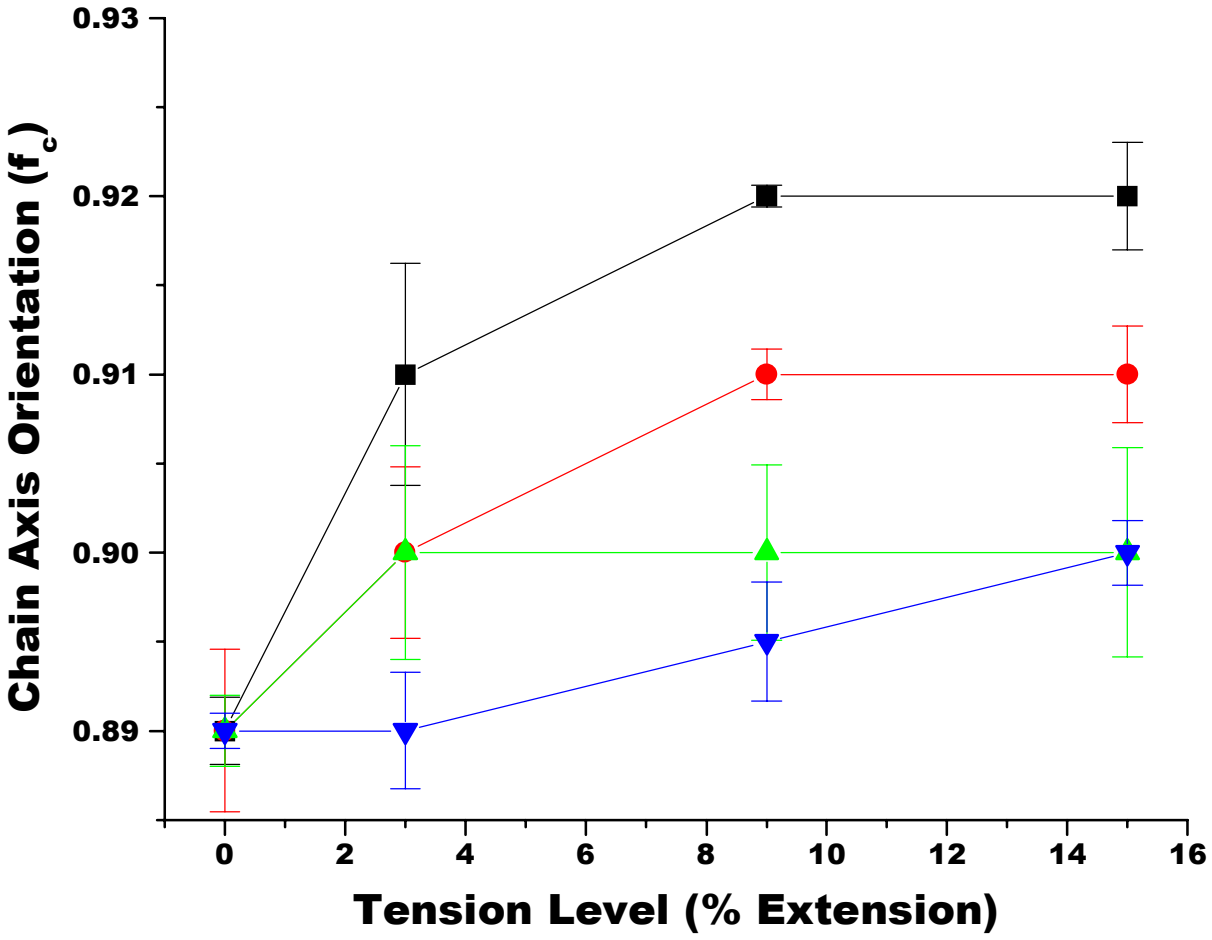

Figure 4.4 Crystalline orientation (f_c) of the A1 films dependence upon annealing tension level and T_a for a t_a of 20min: (-■-) T_a = 205°C, (-●-) T_a = 180°C, (-▲-) T_a = 160°C, (-▼-) T_a = 145°C.

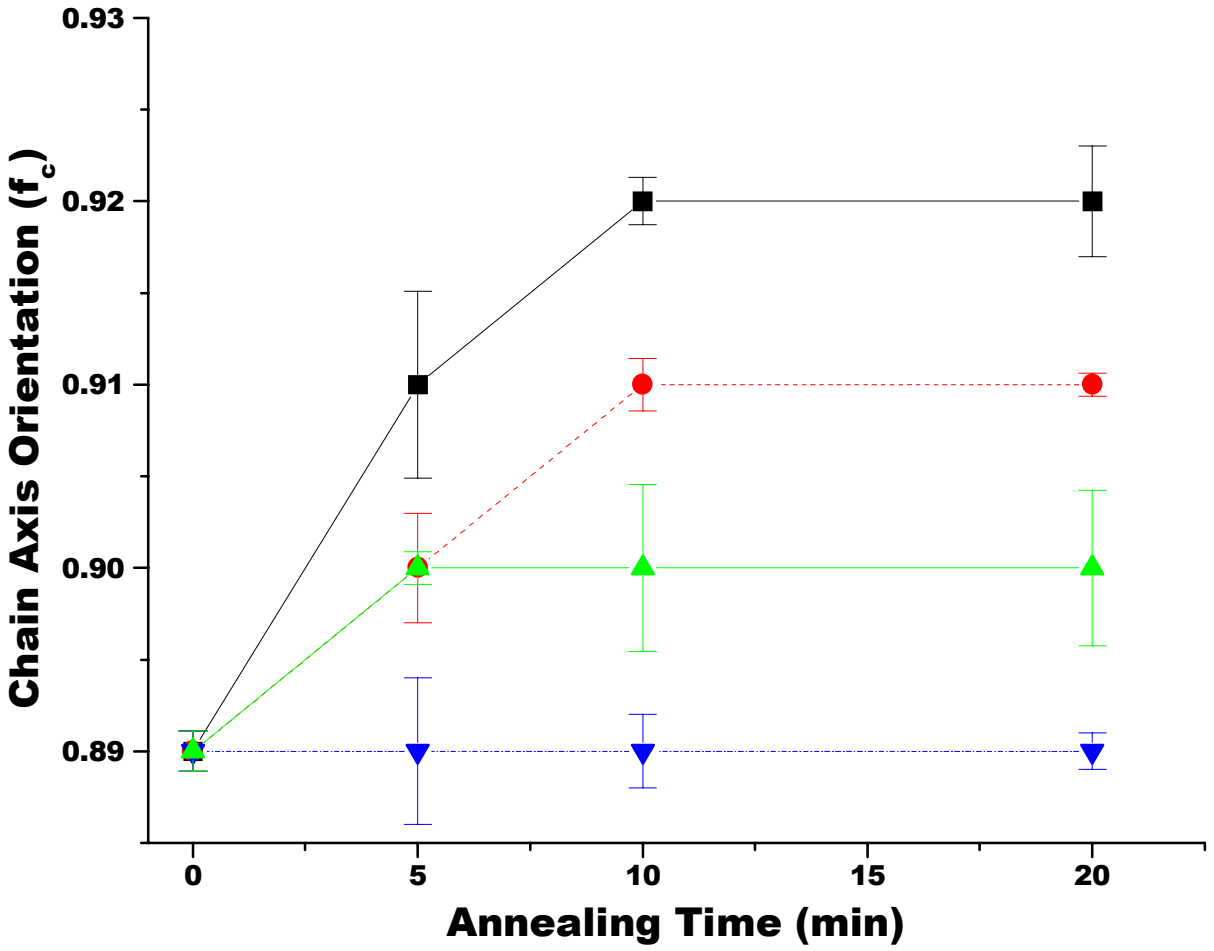

Figure 4.5 Crystalline orientation (f_c) of the A1 films dependence upon annealing tension level and t_a for a T_a of 205°C: (-■-) tension of 15%, (-●-) tension of 9%, (-▲-) tension of 3%, (-▼-) free-annealed (tension of 0%).

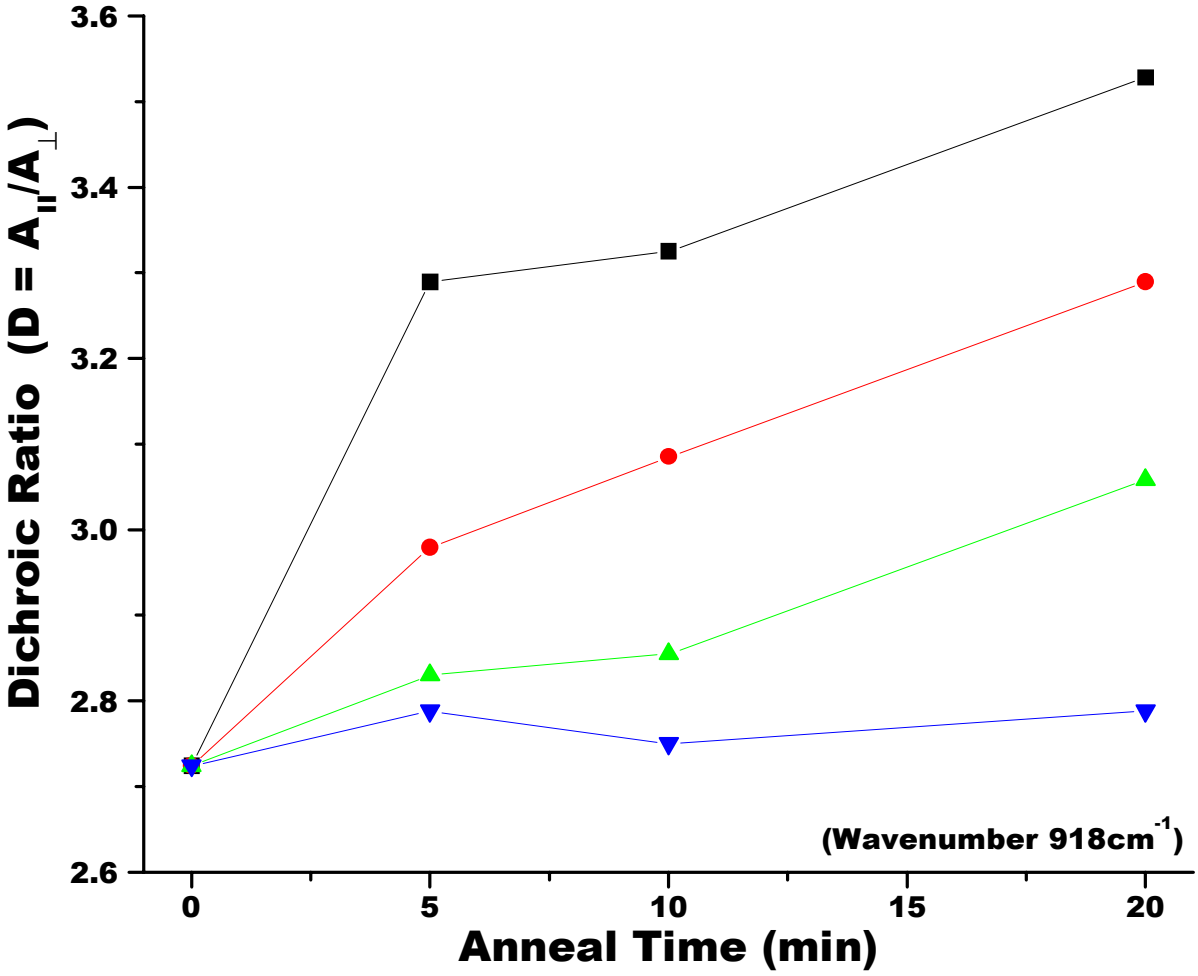

Figure 4.6 The dichroic ratio (D) for the A1 films dependence upon annealing tension level and t_a for a T_a of 205°C using the 918cm^{-1} band: (-■-) tension of 15%, (-●-) tension of 9%, (-▲-) tension of 3%, (-▼-) free-annealed (tension of 0%).

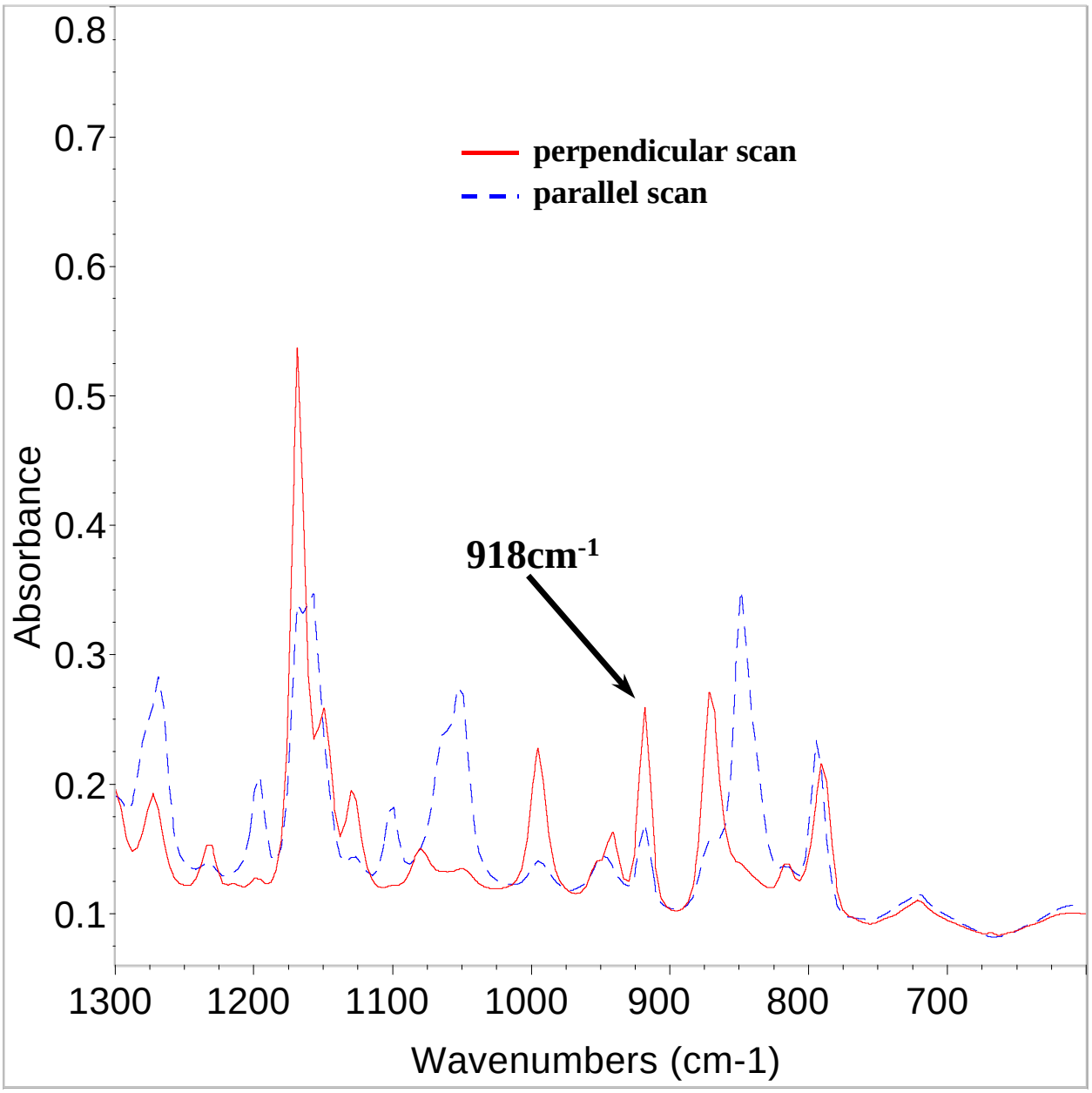

Figure 4.7 The FTIR spectra of the parallel and perpendicular scans for the 918cm^{-1} band obtained on the A1 precursor.

The film morphology was also influenced by the annealing variables as observed in the bulk with TEM after RuO_4 staining as well as on the film surface with AFM. Figures 4.8a-c depicts AFM micrographs of A1 films annealed at 180, 205, and 215°C, respectively, for 20 min. Based upon the morphological analysis of these free-annealed films, it is observed that the stacked lamellar morphology remains intact for the A1 films annealed at 180°C (Fig. 4.8a) and 205°C (Fig. 4.8b). However, the A1 film annealed at 215°C (Fig. 4.8c) has undergone some morphological change. This change appears to be some loss of the well-stacked lamellar structure suggesting surface or larger scale melting. Such large scale melting of the film would not be beneficial for later lamellar separation upon uniaxial deformation in the final stage and thus annealing temperatures were limited to a maximum of 205°C for the main study.

The effect of tension (percent extension) during annealing on the surface morphology is displayed in Fig. 4.9a-c for the A1 films annealed at 205°C for 20 min. The free-annealed specimen corresponding to these conditions was previously presented in Fig. 4.8b. From these micrographs, it is apparent that with increasing extension, lamellar deformation increases. In fact, some distinct lamellar separation has taken place, albeit to a limited extent, at a level of 15 percent tension (Fig. 4.9c) thus creating small surface voids on the order of nanometers (i.e. nano-voids). These are in contrast to the microvoids produced during the later stretching stage. Upon removal of the sample from the annealing oven, those films under tension displayed an observable increase in whitening (haze) that increased with tension level. This is consistent with the AFM findings. The voids induced by tension increase the number of interfaces within the film and as a result a greater fraction of the incident light is scattered and/or reflected. The AFM technique was utilized solely to analyze the surface morphology of the PMP films, and the bulk film morphology may be different from that of the surface.

TEM was also performed on the annealed PMP films after staining with RuO_4. Two representative TEM micrographs of the annealed A1 films are displayed in Fig. 4.10a & b. These micrographs are from two of the same films displayed in Fig. 4.9a-c, i.e. A1 films annealed at a temperature of 205°C for 20 min. using 9 and 15 percent extension, respectively. It is evident upon examination of these TEM micrographs that the lamellae become somewhat deformed as the extension level during annealing increases. These findings validate the AFM surface results and further suggest that there is no difference between the bulk and surface morphology. This is not surprising since a previous HDPE[2] investigation noted that there is no difference between the surface and bulk morphologies, where those samples were also extruded to film thickness ca. 1 mil.

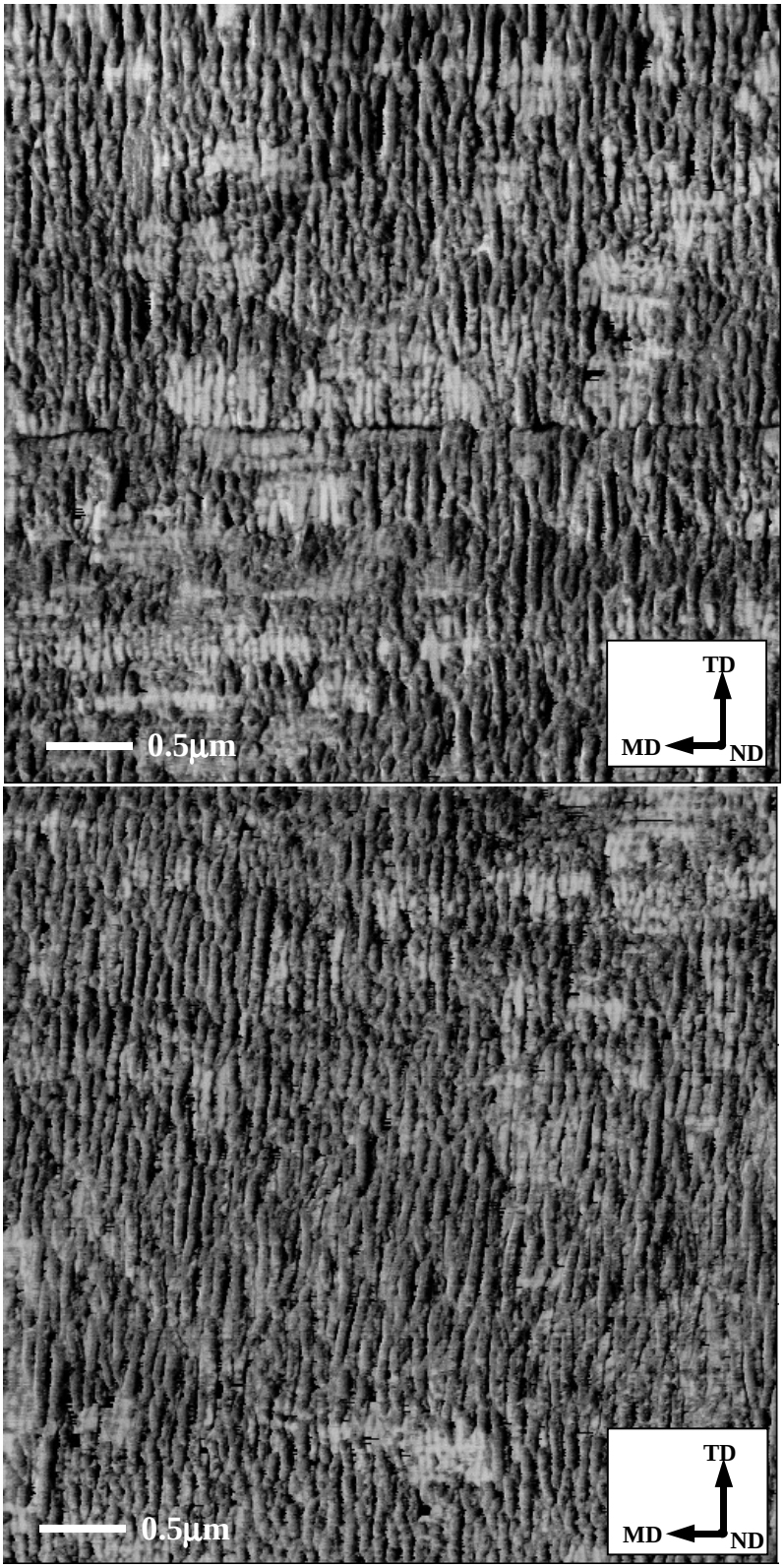

Figure 4.8 AFM phase images of the A1free-annealed films with t_a equal to 20min. a) T_a = 180°C, b) T_a = 205°C, and c) T_a = 215°C. The MD is labeled. The images are 3µm x 3µm.

c)

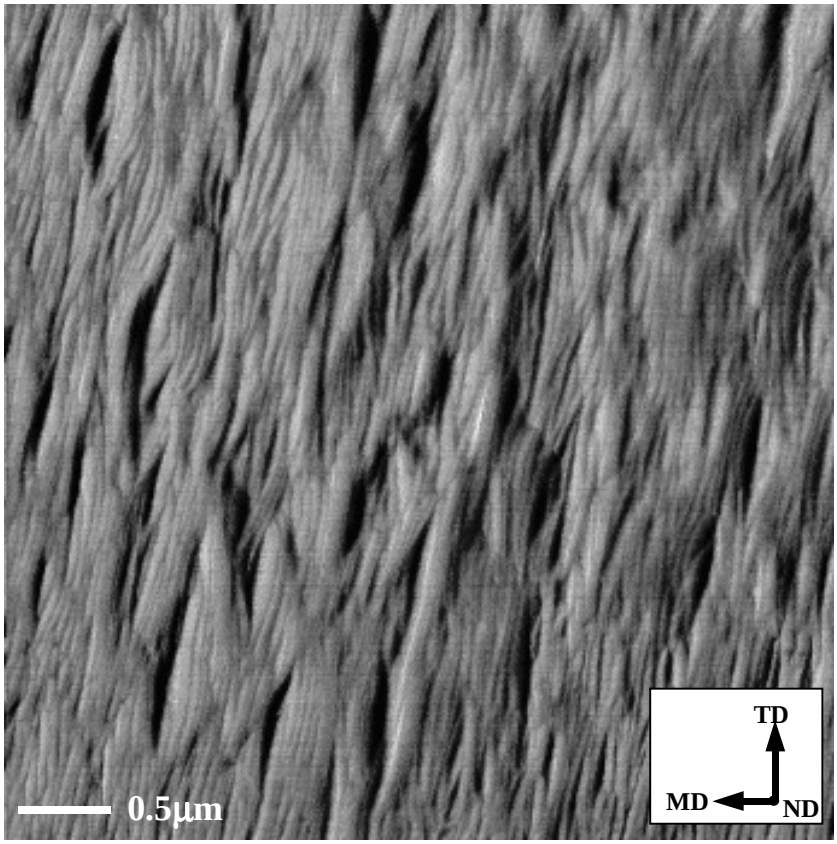

(Figure 4.8 cont'd)

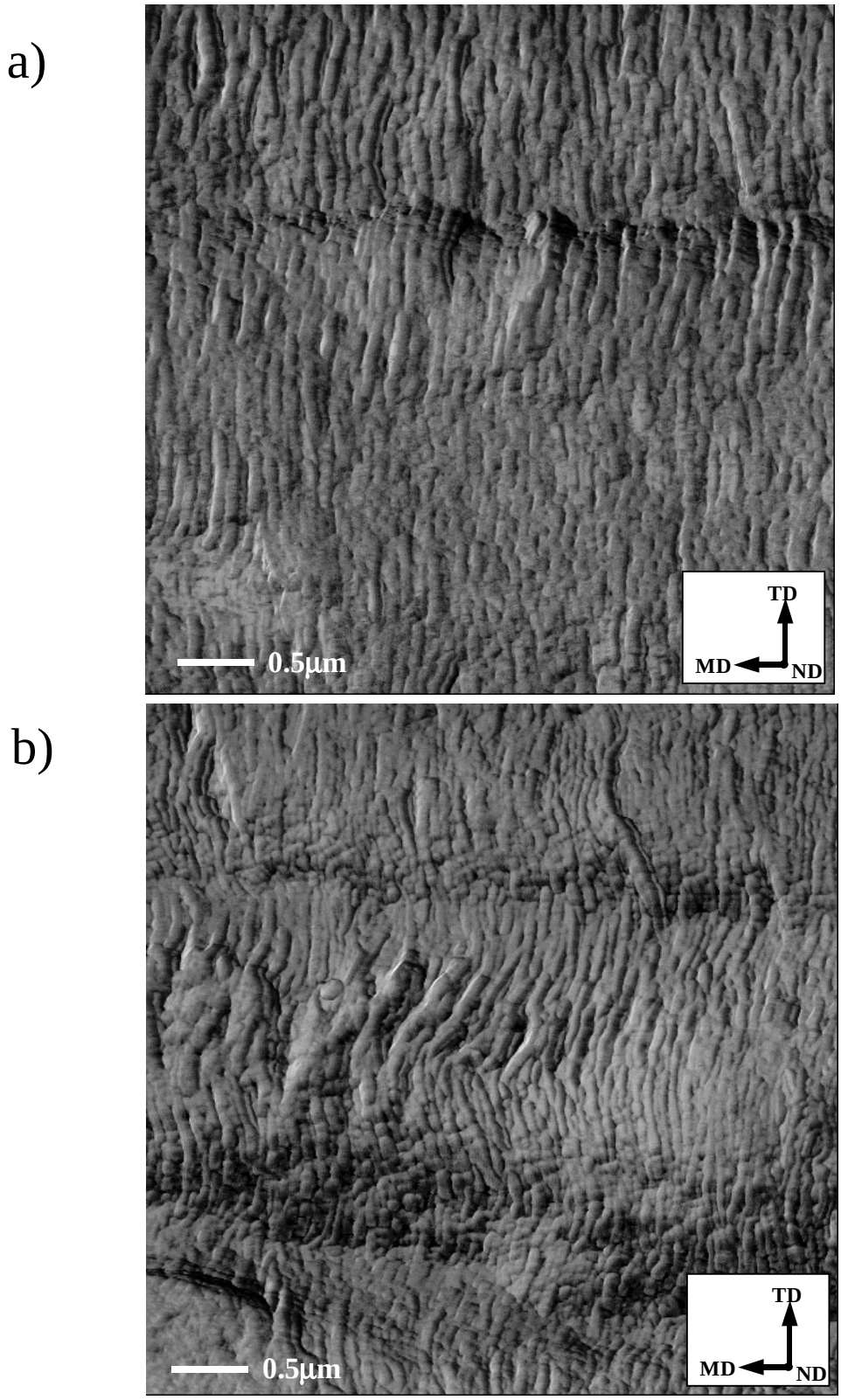

Figure 4.9 AFM phase images displaying the influence of tension during annealing on the morphologies of selected A1 films where T_a = 205°C & t_a = 20min. a) 3% tension, b) 9% tension, and c) 15% tension. The MD is labeled. Images are 3μm x 3μm.

c)

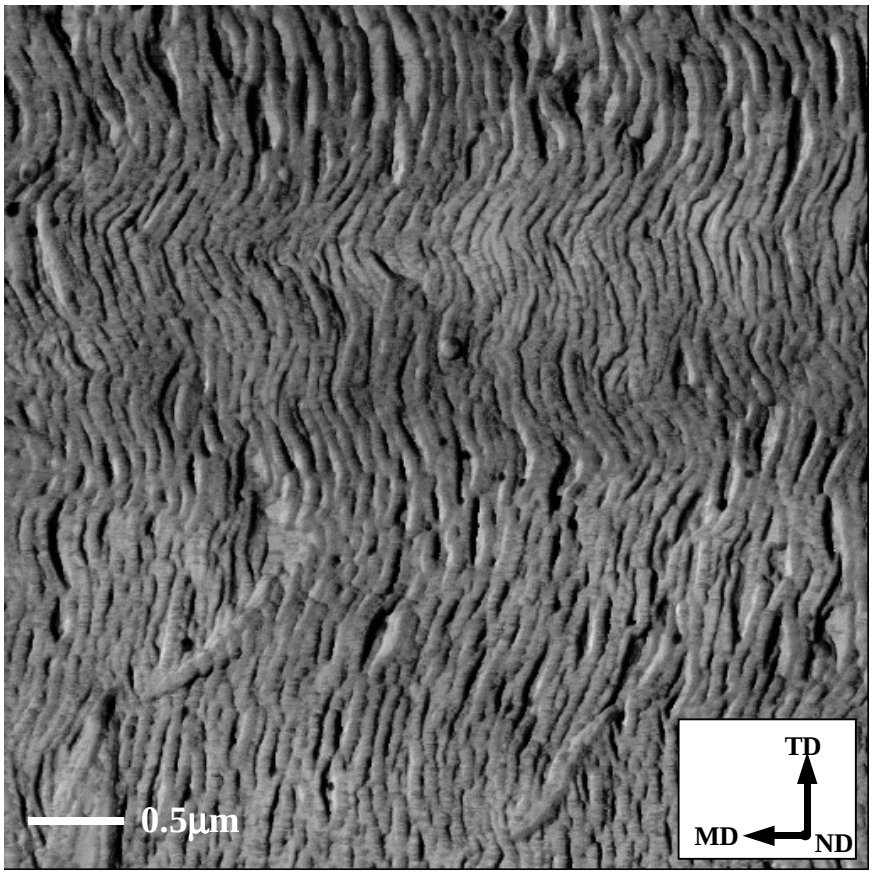

(Figure 4.9 cont'd)

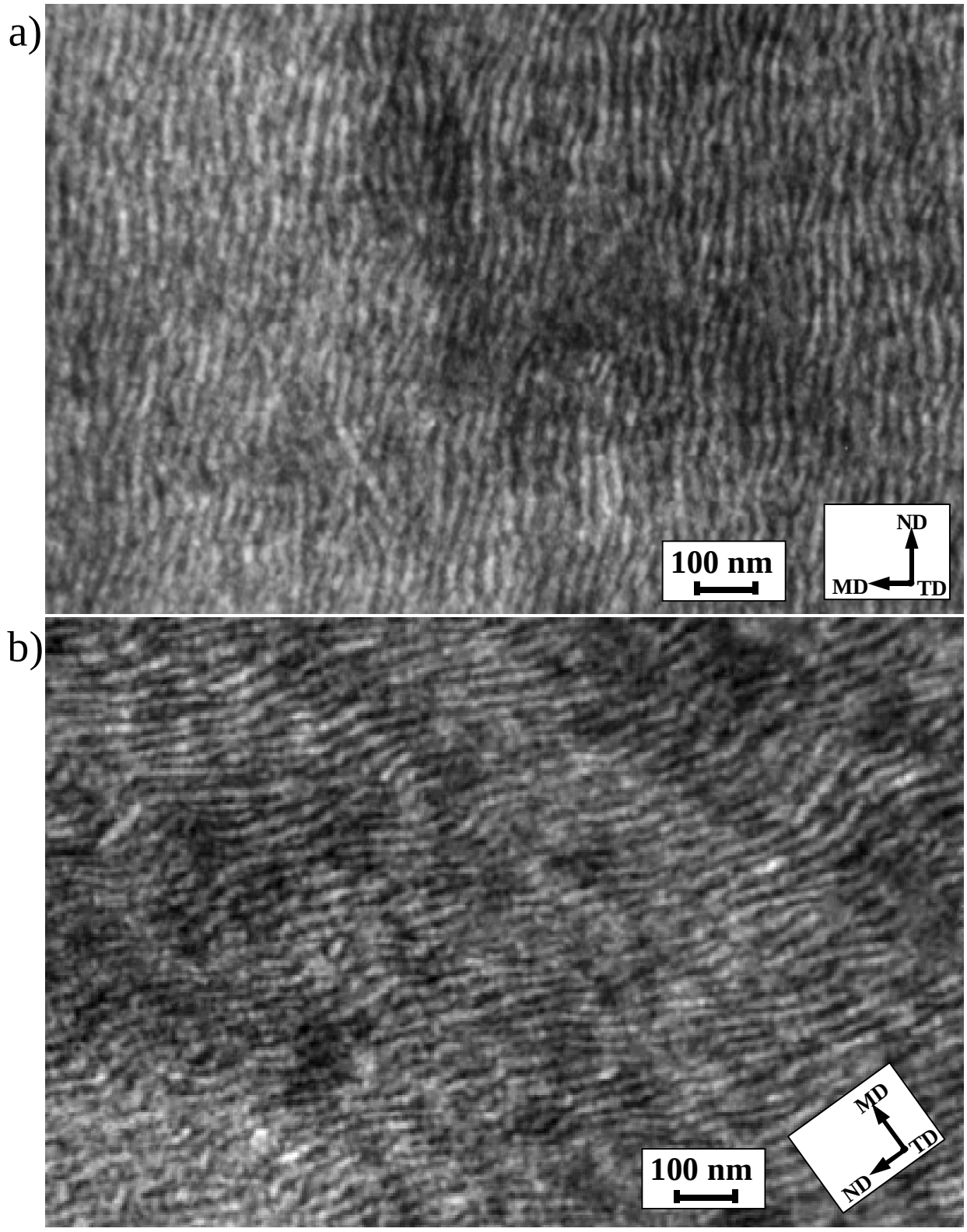

Figure 4.10 TEM micrographs of RuO stained A1 annealed films where T_a =205°C & t_a = 20min. a) 9% tension and b) 15% tension. The MD is shown.

For all the A1 films, the effect of tension level during annealing had no apparent consequence on the level of crystallinity or the crystalline melting point for a constant annealing temperature and time. In contrast, both annealing temperature and time did influence these same two properties. The melt temperature appears to be slightly enhanced by annealing temperature and time as shown in Table 4.3. These results are for selected samples where the reader will note the measured lack of influence tension has on either film property (T_m or X_c) versus the effect of the annealing temperature and time.

Table 4.3 Pertinent film characteristics of selected A1 annealed films.

T_a (°C)	160	205	205	205	205	205
t_a (min)	20	10	20	20	20	20
% tension	free	free	free	3	9	15
T_m (°C)	230	230	233	232	232	233
X_c (%)	65	67	71	69	70	71
f_c	~0.89	~0.89	~0.89	0.91	0.92	0.92

Similar results are shown in Fig. 4.11, where the full DSC scans are displayed for three specific A1 films. A rather sharp melting peak characterizes each scan, including the precursor. The melting peak of each annealed film has shifted by approximately the same amount, regardless of tension level. In this figure, each annealed film presented had utilized a temperature of 205°C for 20min. The remainder of the annealing results for the resin A and resin C films were comparatively similar as those presented. Both the crystallinity and melting point of the resin B films were not determined for the annealed films. This was due to the presence of multiple melting peaks upon annealing, as can be observed in Fig. 4.12, where the multiple melting peaks are likely a consequence of the higher comonomer content present in resin B (ca. 6.5 wt%). In this figure, the DSC heating traces of three B1 films are presented: the precursor, a free-annealed film, and a film annealed under 15 percent tension where the two latter films were annealed at 205°C for 20 min.

The annealing temperature and time have also been observed to affect the relaxation attributed to crystalline mobility (α_c relaxation).[10,16,28] In the case of our PMP films, the magnitude of the overall relaxation decreased as a function of crystallinity. This behavior is displayed for three A1 films, including the precursor, in Fig. 4.13. Additionally, it was recognized that as the crystallinity increases, the temperature associated with the maximum in the α_c relaxation (termed $T_{\alpha c}$) shifted to higher values. In contrast, the relaxation associated with

cooperative segmental mobility (T_g relaxation) decreased in overall magnitude for the film annealed at the higher temperature (205°C) as a result of the higher crystallinity. For the film annealed at 160°C for 20 min, a small crystallinity increase occurs, but the T_g relaxation remained constant. As shown in Fig. 4.14, the effect of tension did not appear to systematically alter the overall magnitudes of either the α_c or T_g relaxations or the temperatures associated with the maximum in the PMP relaxations. These findings are in contrast to a report[26] that determined there was an influence of uniaxial draw ratio on the PMP relaxations, where in that investigation a maximum draw ratio of 6 was utilized. Thus, the lack of a systematic effect observed in our case is likely the consequence of the low tension levels utilized. The α_c and T_g relaxations of the resin C films were comparable to those of resin A with respect to both changes in magnitude and $T_{\alpha c}$ with crystallinity. As was previously shown, the mechanical relaxations of the resin B films did not systematically change and were also difficult to analyze due to the convoluted nature of the α_c and T_g relaxations. Thus, no DMS data is presented regarding this resin. It will be shown in the next section, which addresses the stretching results, that the convoluted α_c relaxation characterizing the resin B films has adverse consequences on the formation of microporous membranes.

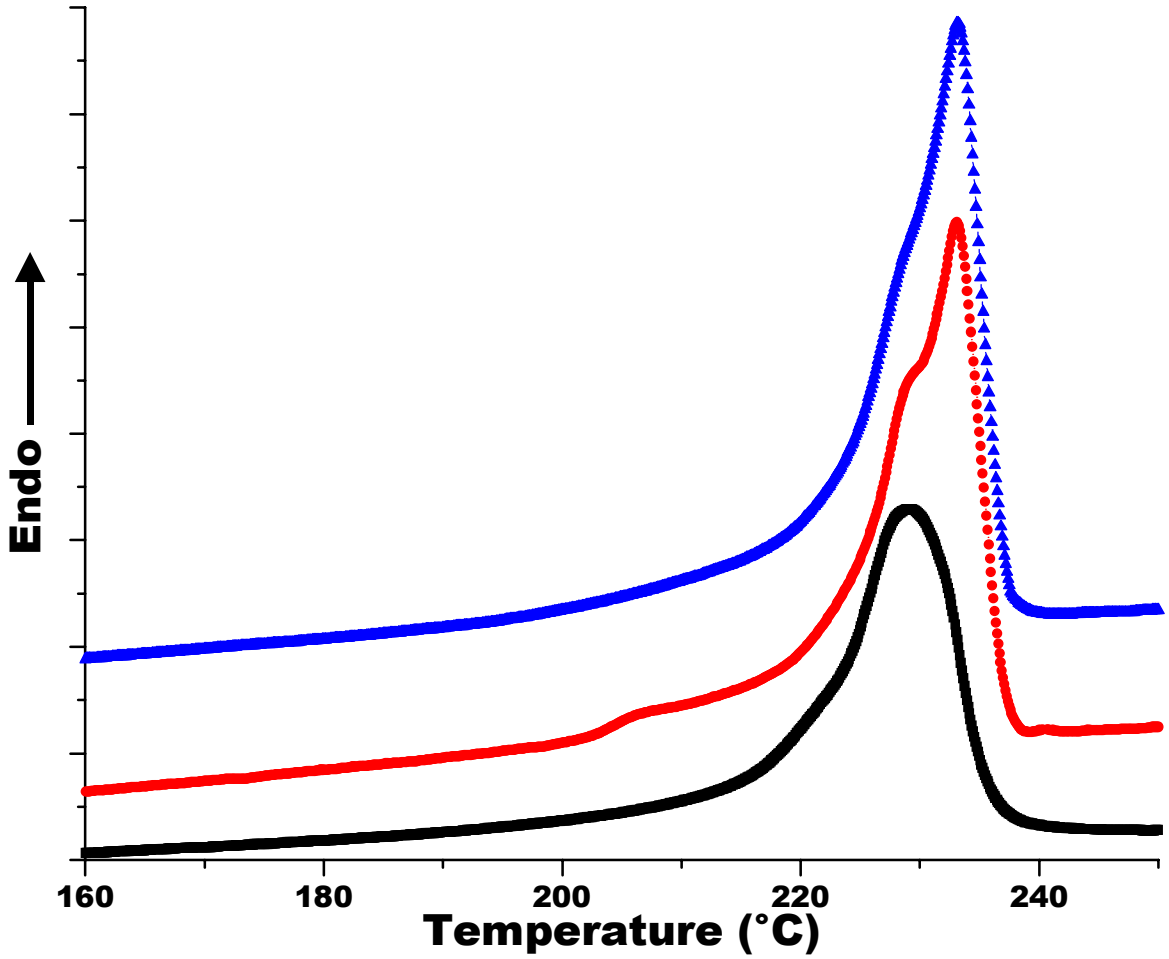

Figure 4.11 DSC heating scans of theA1 precursor and annealed films (T_a =205°C for t_a=20min): (-■-) precursor, (-●-) free annealed, and (-▲-) 15% tension utilizing a heating rate of 30°C/min.

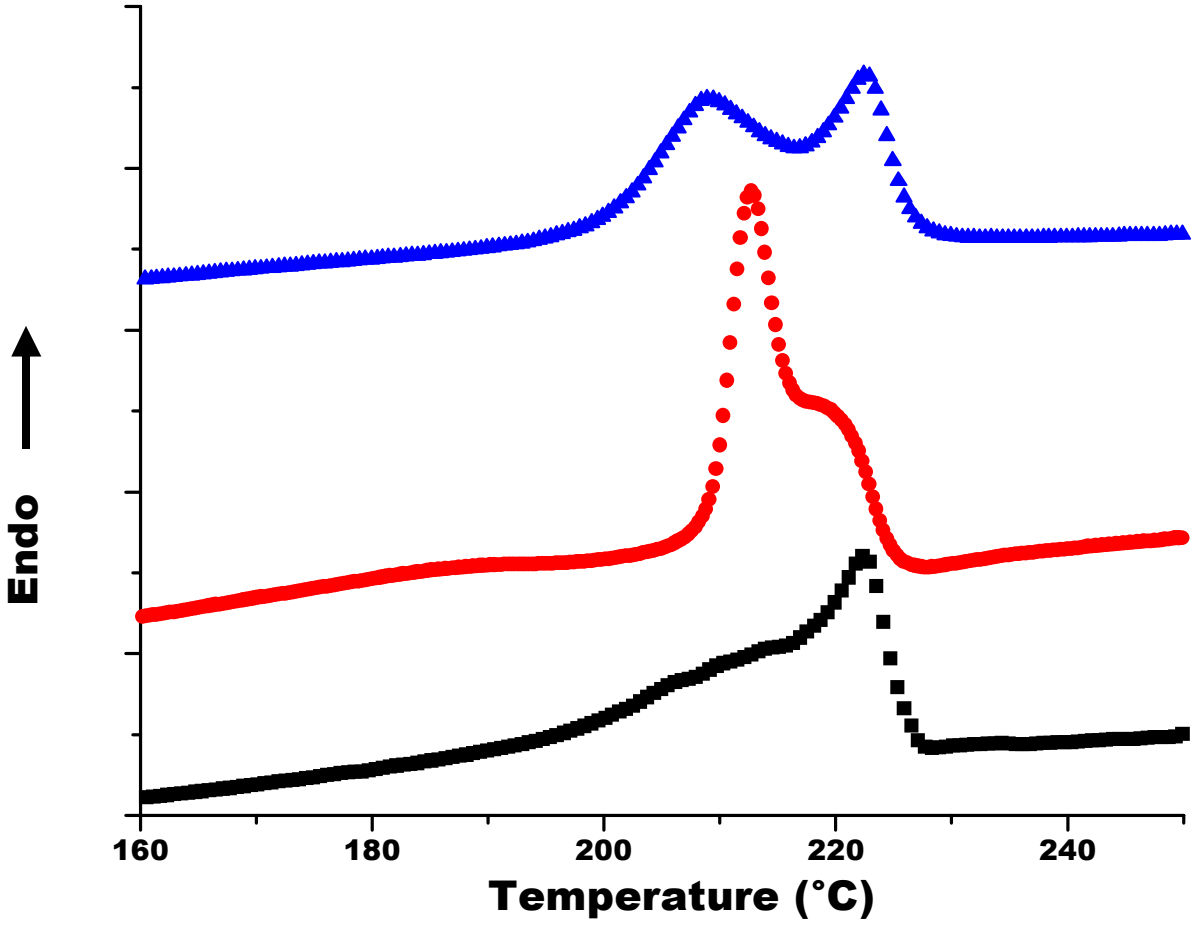

Figure 4.12 DSC heating scans of the B1 precursor and annealed films (T_a =205°C for t_a=20min): (-■-) precursor, (-●-) free annealed, and (-▲-) 15% tension utilizing a heating rate of 30°C/min.

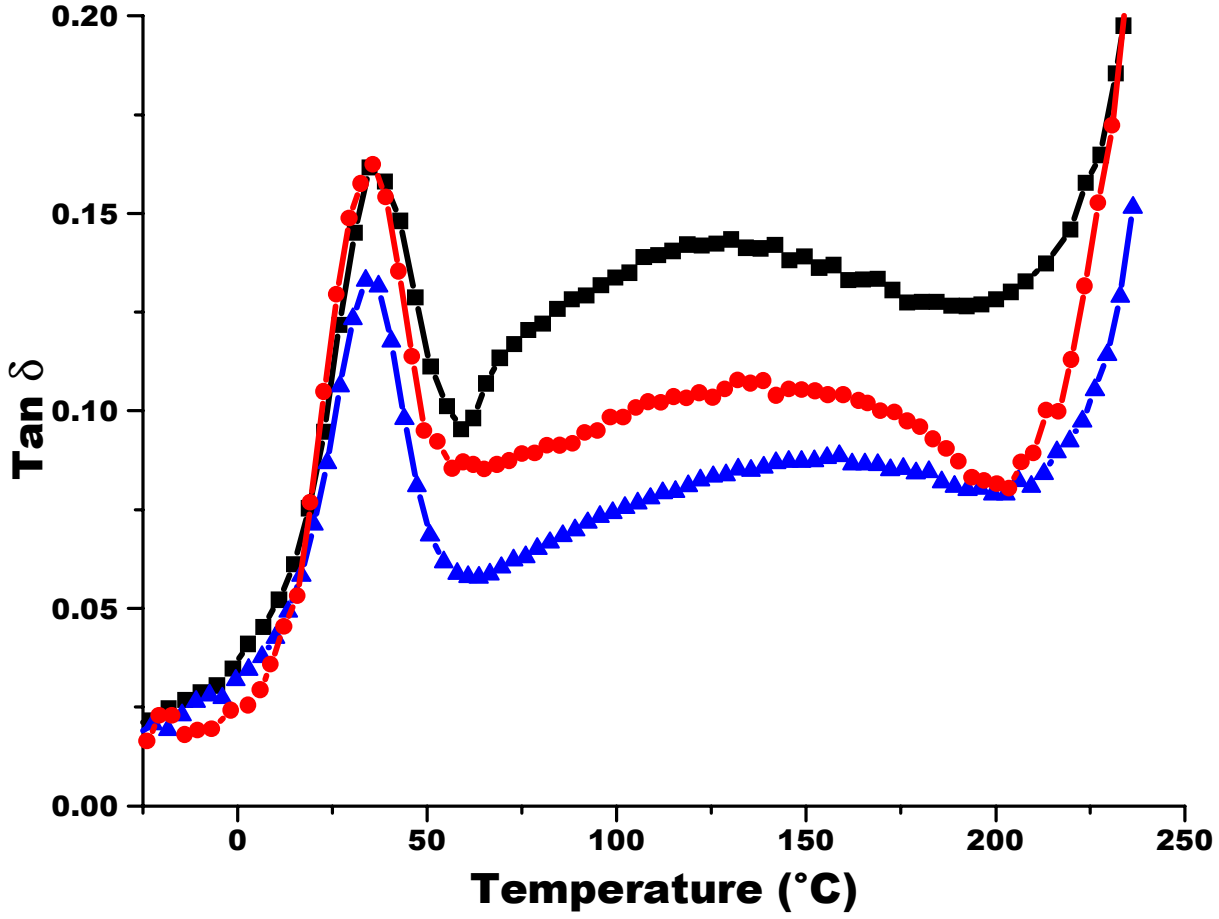

Figure 4.13 Tan δ as a function of temperature for the A1 precursor and annealed films (t_a=20min): (-■-) precursor, (-●-) T_a = 160°C, and (-▲-) T_a = 205°C. This data was obtained utilizing a heating rate of 2°C/min and a frequency of 1.0 Hz.

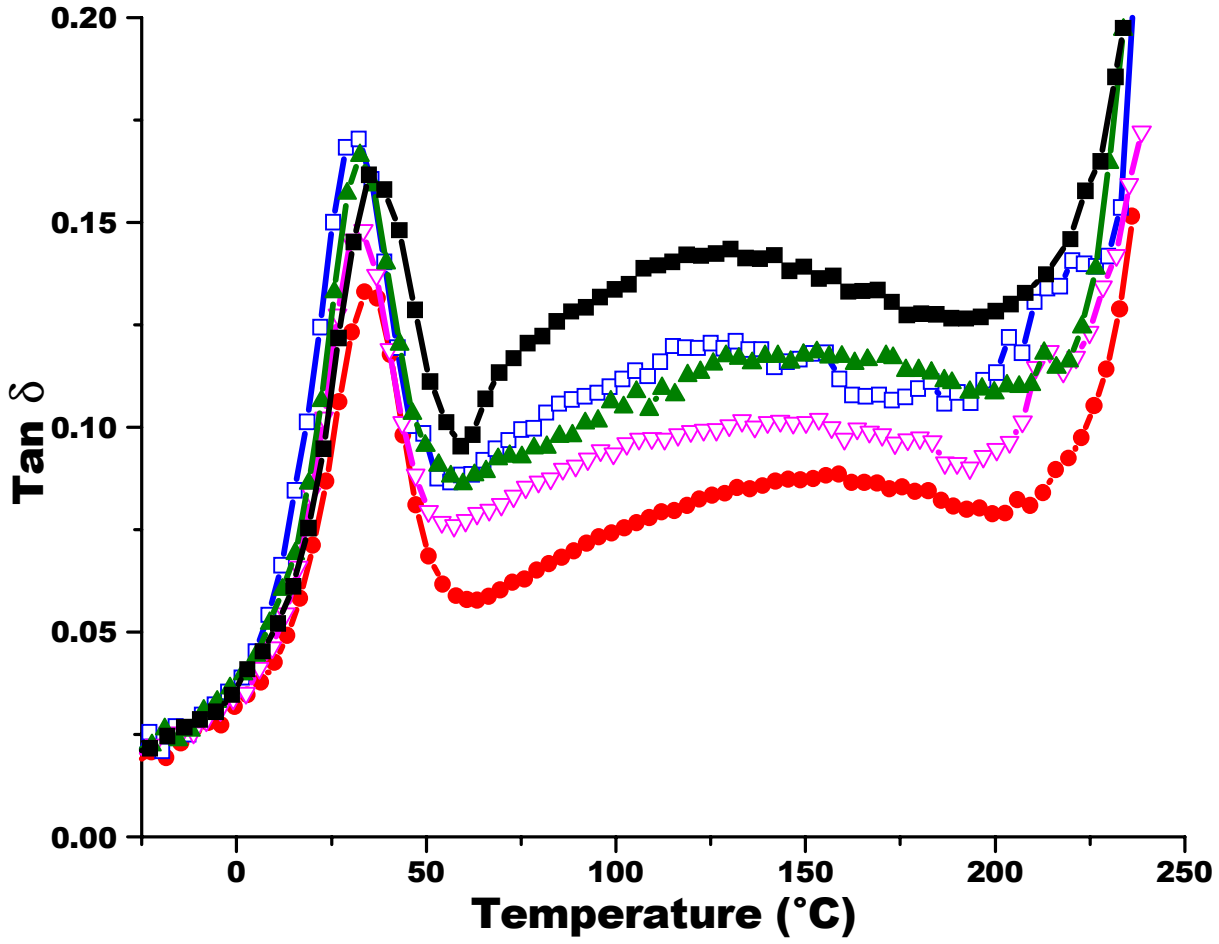

Figure 4.14 Tan δ as a function of temperature for the A1 precursor and annealed films (T_a = 205°C and t_a=20min): (-■-) precursor, (-●-) free-annealed, (-□-) 3% tension, (-▲-) 9% tension, and (-▽-) 15% tension . This data was obtained utilizing a heating rate of 2°C/min and a frequency of 1.0 Hz.

4.3-2 Microporous Development by Stretching (Stage Three):

The annealed films were subjected to the two step stretching procedure described earlier. Besides the crosshead speed, which was kept constant throughout the entire study at 150 mm/min, the variables of temperature and extension level were considered for each step. The cold stretch temperatures studied were 40°C (approximately equal to the PMP T_g [27]), 70, 80, and 90°C with extension levels (%CS) equal to 50, 65, 80, and 90 percent. The hot stretching temperatures utilized were 120, 160, and 180°C while the levels of extension (%HS) were 50, 65, 80, and 90 percent. The levels of extension were calculated using Eqn. 4.4.

$$\%\ \text{Extension} = \frac{l_f - l_o}{l_o} \times 100\% \qquad \text{(Eqn. 4.4)}$$

where l_f is the final length of the film after the cold or hot stretch step while l_o is the initial length of the film *prior to any cold stretching*.

Immediately after the hot stretching step, a relaxation/heat-setting step was employed in the MEAUS process. In this study, the relaxation/heat-setting step occurs at the same temperature as hot stretching where relaxation amounts equal to 0, 20, and 40 percent were investigated while the heat-setting time was held constant at 10 minutes.

From the above, it clear that the possible number of annealing/stretching combinations is large, but the authors do not want to give the impression that every combination was attempted. Instead, the samples reported here will represent the general findings and will be based on a standard set of annealing and stretching conditions. The standard annealing/stretching variable combination, hereafter referred to as the *standard condition*, consists of a precursor that is free-annealed at a temperature equal to 205°C for 20 min, followed by cold stretching at 70°C to 50 percent extension, then hot stretching at 160°C to 90 percent extension without any relaxation (0%). A nomenclature for designating the final film histroy is employed, which utilizes the starting precursor label along with any annealing and/or stretching variable that was altered from the standard condition. For example, if an annealed A1 film was cold stretched at a temperature equal to 40°C instead of 70°C, the final stretched sample would be labeled A1-T_{cs}40. It would be assumed that the other annealing and stretching conditions were analogous to the standard variable combination.

In this section, numerous process variable combinations will be presented with regard to their influence on final film morphology and permeability (inverse function of Gurley number). These combinations will include the melt-extruded precursor morphology and f_c value; the annealing temperature, time, and tension level (percent extension); the cold stretch temperature

and percent extension, as well as the hot stretch temperature and percent extension. The resin A precursor films A1 and A2 were mainly utilized to investigate the effects of these variable combinations and thus the forthcoming results will focus largely upon these materials. Extensive annealing and stretching variable combinations were also employed on the resin B and C films. Selected results from these latter studies will be addressed following those of resin A.

The effect of the annealing variables on the membrane permeability and morphology will be presented first. In Fig. 4.15, the Gurley number dependence on annealing temperature for the stretched films from precursors A1 and A2 is shown. Recall that other than annealing temperature, the remainder of the standard annealing/stretching condition was kept constant for the stretched films presented in this figure. It is observed that the Gurley number decreased with increasing annealing temperature for both the resin A films A1 and A2. Additionally, note that the A1 stretched films possess lower average Gurley numbers than do the comparable A2 stretched films, i.e., those films annealed and stretched at similar conditions. The reader may recall that the precursor A1 had an f_c of 0.89 while that of the precursor A2 was 0.83. This latter result suggests that membrane permeability also increased with higher crystal orientation. While not presented here, when equivalent stretching conditions were used, it was found that film rupture during stretching occurred more frequently for films annealed at a lower temperature compared with films annealed at a higher temperature. Further, annealing time played an important role in the frequency of film rupture during stretching. Specifically, the shorter the annealing time, the more often the film broke during stretching.

Annealing time also influenced the membrane permeability, as shown in Fig. 4.16, where the Gurley number dependence on annealing times of either 10 or 20 minutes for A1 and A2 stretched films is displayed. In this figure, it is seen that the Gurley number is higher for either stretched A1 or A2 films annealed at the shorter of the two times. Data from experiments utilizing a 5 minute annealing time which are not displayed here, were found to produce permeable stretched films but with substantially higher Gurley numbers (lower permeability) than the final films annealed at either 10 or 20 minutes, all other variables remaining constant. It is noted that the A1 final film possesses a lower Gurley value than does the A2 stretched film for equal annealing/stretching conditions. For example, the Gurley number of the membrane A1-t_a20 equals 33 seconds while that of A2-t_a20 equals 79 seconds. The reader may recall that Gurley numbers less than 100 sec. characterize a “quality” microporous film. Thus, Fig. 4.16 indicates, three such membranes were achieved.

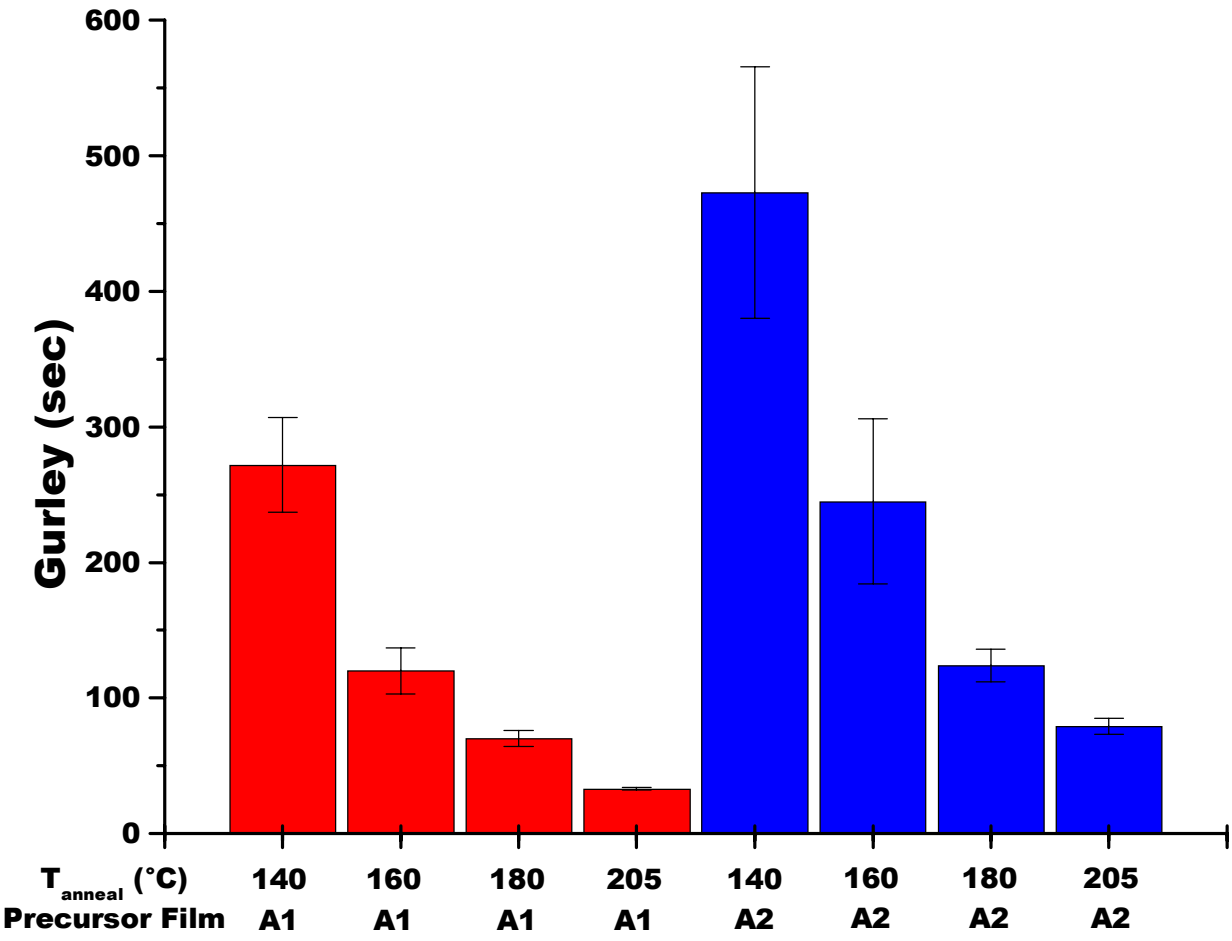

Figure 4.15 Effect of annealing temperature on the Gurley number for A1 and A2 stretched films. The other annealing/stretching parameters remained constant with the standard condition.

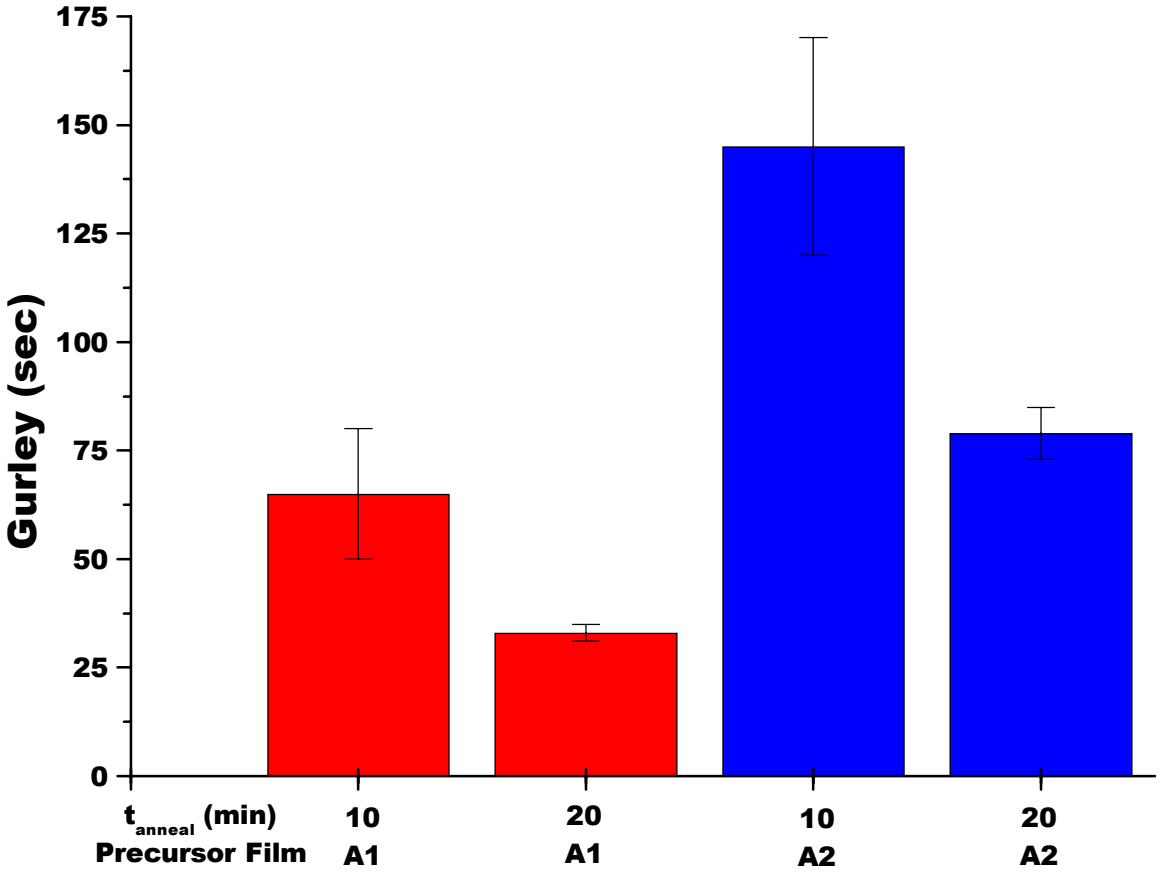

Figure 4.16 Effect of annealing time on the Gurley number for A1 and A2 stretched films. The other annealing/stretching parameters remained constant with the standard condition.

The remaining annealing variable, tension (percent extension), was shown earlier to influence the morphology of the annealed film, thus, it was to be expected to alter the microporosity and permeability of the final stretched film. Indeed, this is true, as observed in Fig. 4.17 which displays the Gurley number as a function of the tension level during annealing for the films from precursors A1 and A2. In either case, it is recognized that with increasing tension, the Gurley number increases. In fact, when a tension level of 15 percent was utilized, the Gurley number for either stretched film from A1 or A2 was equal to or greater than 1000 seconds indicating an essentially impermeable film. The morphologies, as viewed with AFM, are shown in Fig. 4.18a-d for selected A1 membranes, specifically, A1-%ext0 (standard condition), A1-%ext3 and A1-%ext9, respectively. There is detectable microporosity to varying degrees in these films. The finer structure of a PMP final film can be observed in Fig. 4.18d, which is an AFM micrograph of the same membrane shown in Fig. 4.18a, accept at higher magnification. Note the interlamellar fibers are oriented parallel to the MD and stretching direction or perpendicular to the lamellae. The stretched film morphologies of A1-%ext0 and A1-%ext3, Figs. 4.18a & b, respectively, are roughly identical, both possess relatively large microporous structures. The stretched films annealed under higher levels of tension, A1-%ext9, Fig. 4.18c, display deformed microporous morphology. The membrane A1-%ext15, not shown here, possessed little if any microporous character, explaining the reasoning behind its measured Gurley number of approximately 1000 seconds. In order to possess a low Gurley number, the microporosity must also occur throughout the *entire cross-section* of the stretched film, as is revealed via SEM in Fig. 4.19. This figure is a SEM micrograph of the A1 membrane produced using the standard annealing/stretching condition, where the film is viewed along its transverse direction (TD), which is in contrast to the normal direction (ND) utilized for the AFM micrographs.

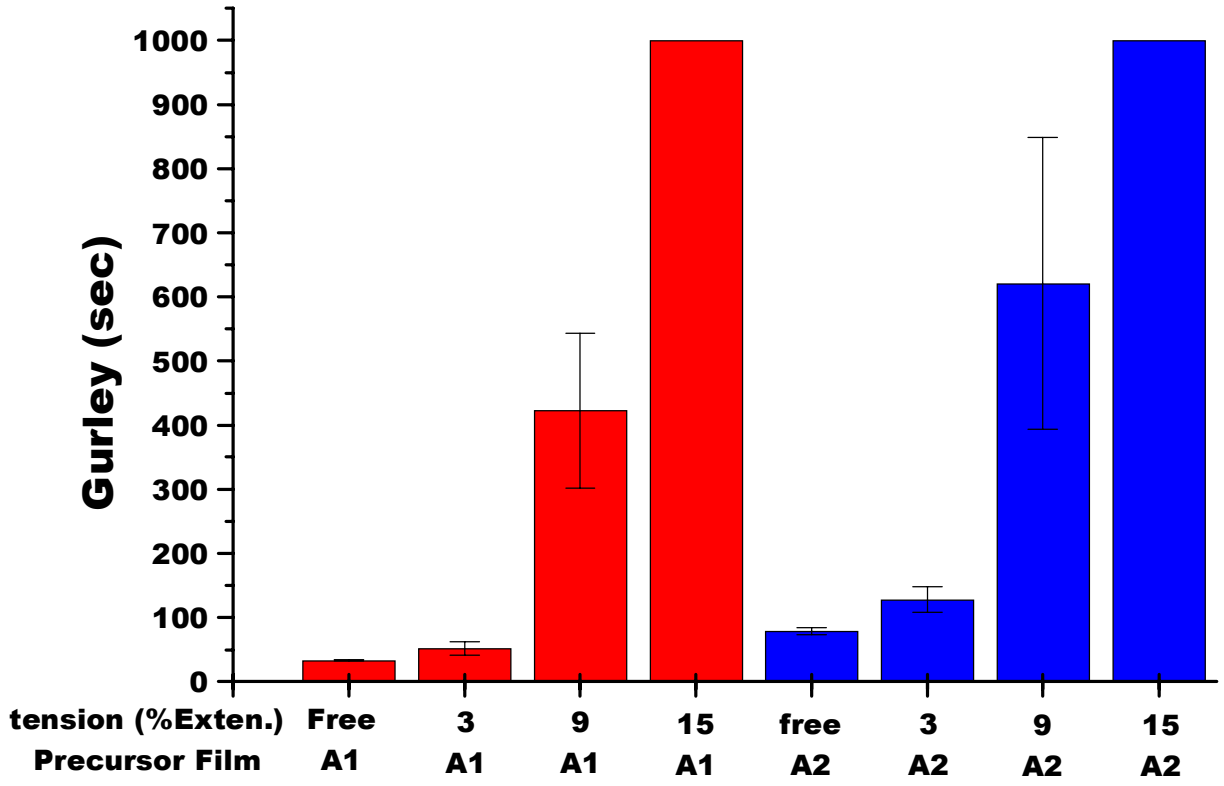

Figure 4.17 Effect of tension level during annealing on the Gurley number for A1 and A2 stretched films. The other annealing/stretching parameters remained constant with the standard condition.

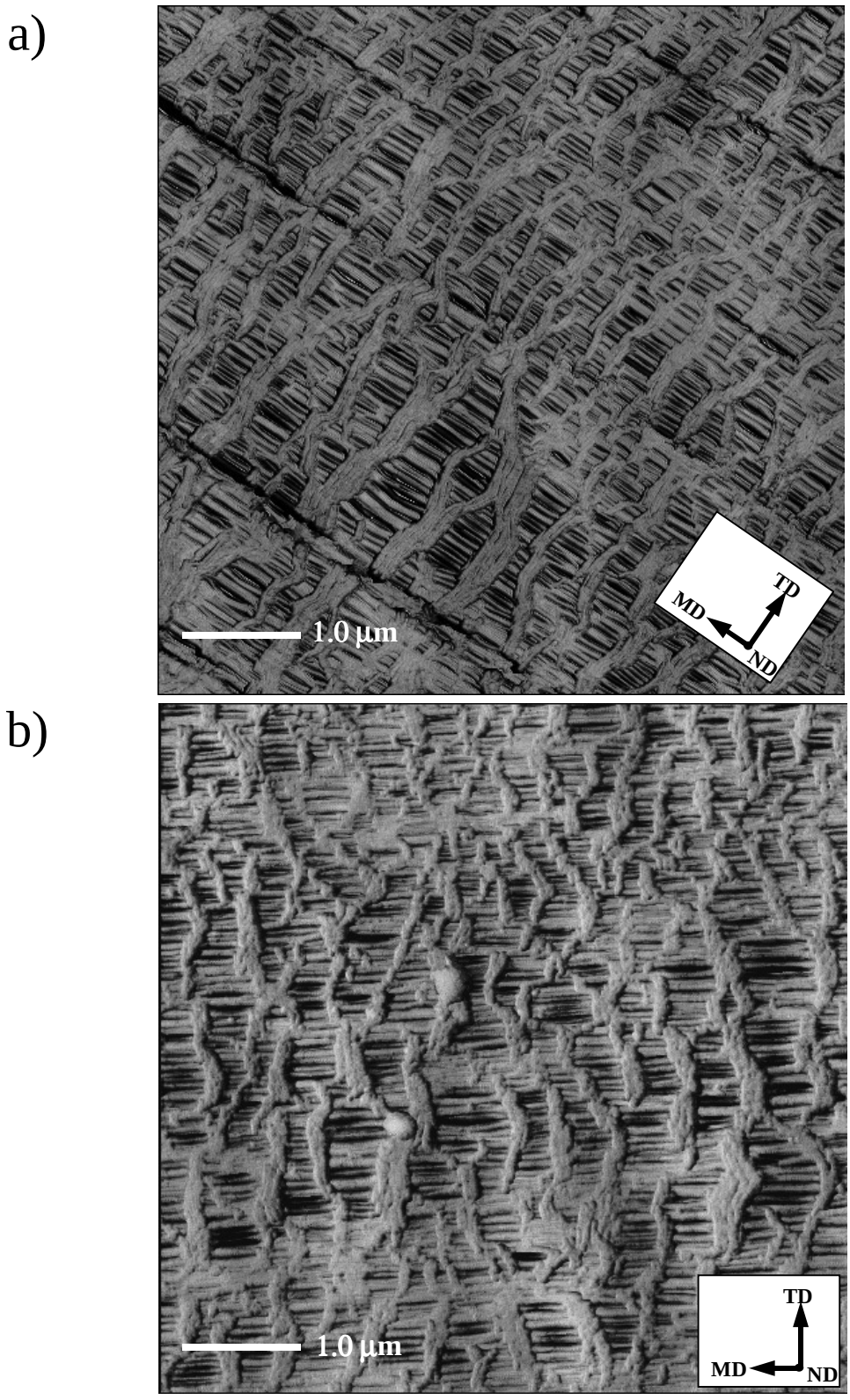

Figure 4.18 AFM images displaying the influence of annealing tension on stretched A1 membranes where T_a = 205°C & t_a = 20min. a) free, b) 3% tension, c) 9% tension, and d) free but at higher magnification than a. The MD is labeled.

c)

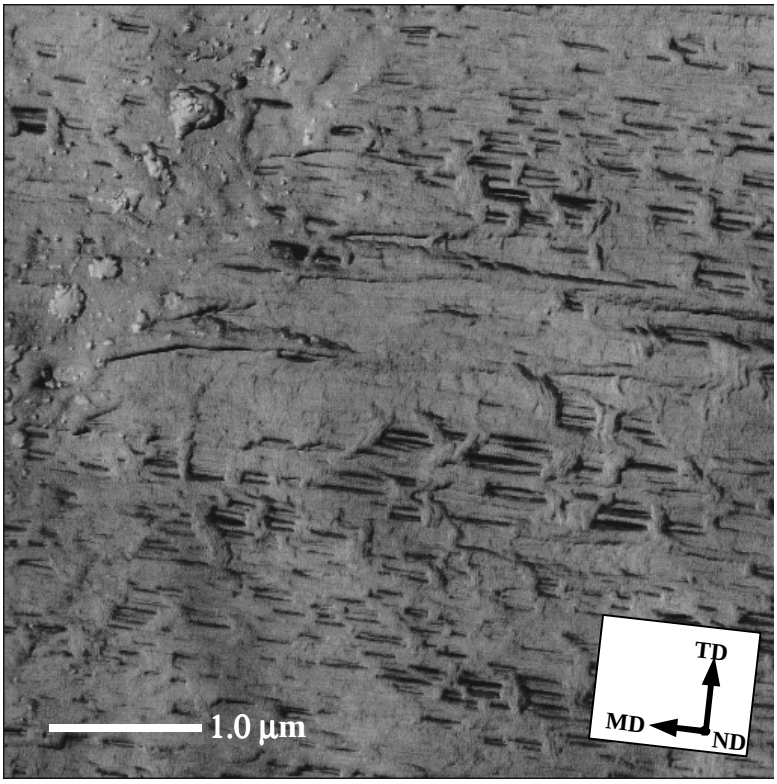

d)

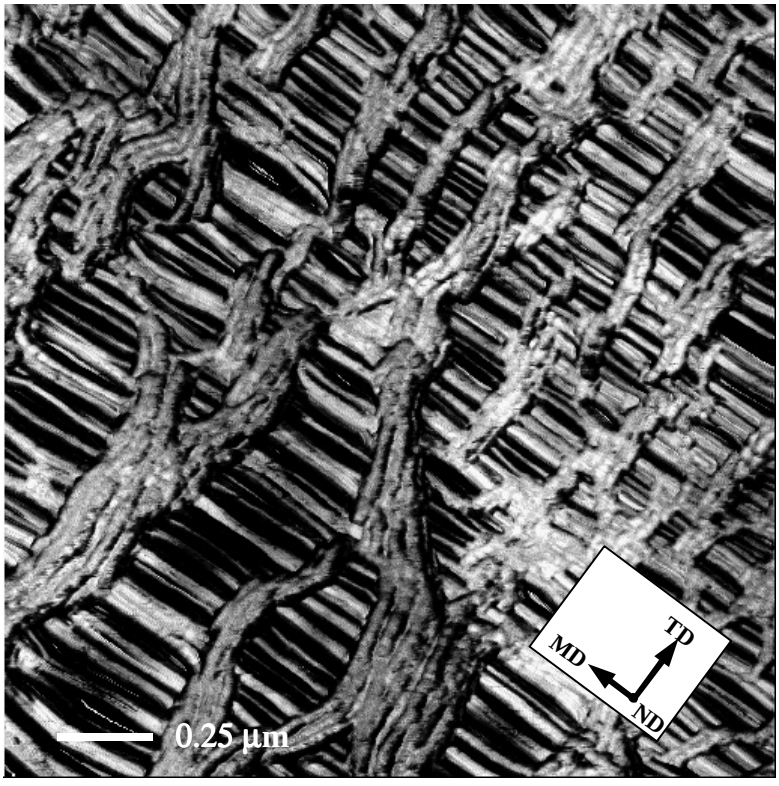

(Figure 4.18 continued)

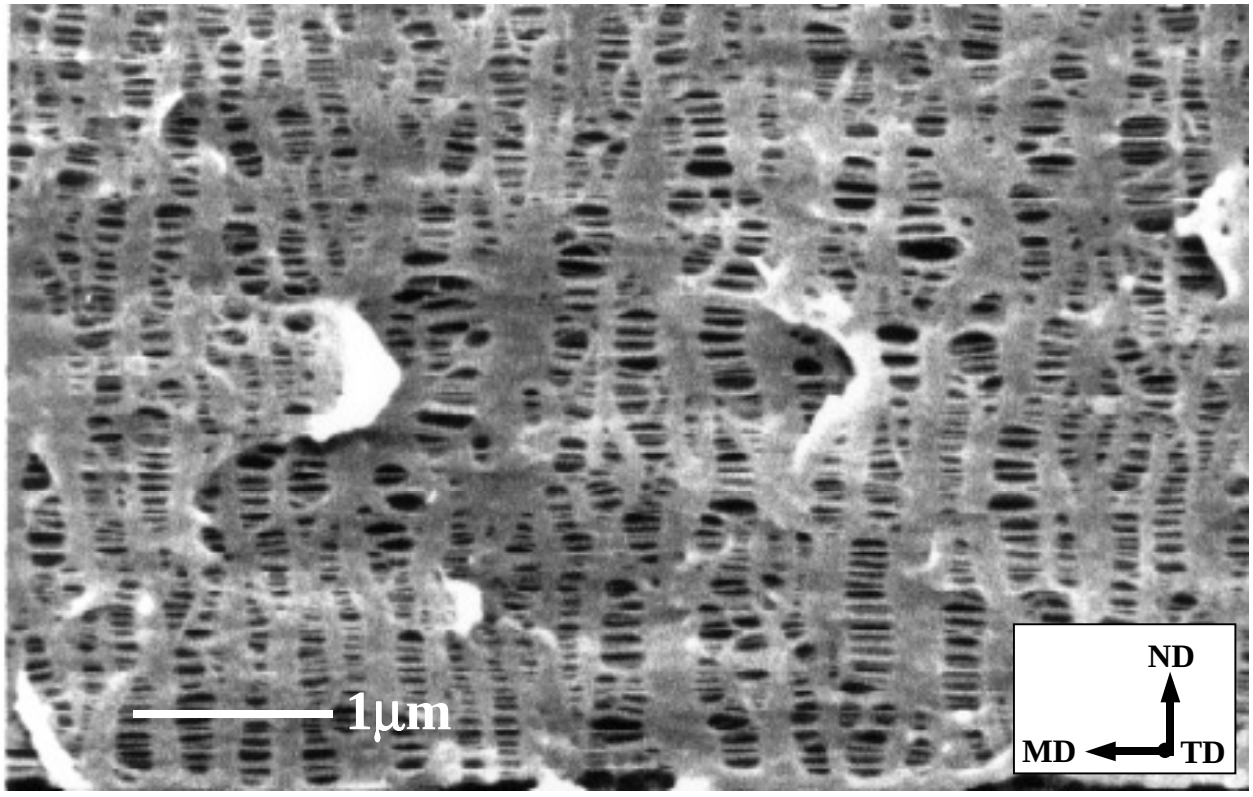

Figure 4.19 SEM micrograph of the cross-section of the A1 membrane produced using the standard annealing/stretching condition.

We now address the effect the cold stretch parameters, T_{cs} and %CS, have on the final film microporous structure and permeability. Since we have established that the annealing/stretching results from precursor A2 parallel those from A1, except that a lower permeability is obtained for the A2 membranes, the remaining resin A data will only consider results from film A1. Figure 4.20 is a plot of the Gurley number as a function of the level of cold stretch extension. Each plot also provides results for a constant value of cold stretch temperature. It is recognized that as the specific extension level was increased from 50 to 90 percent, the membrane Gurley decreased. However, if the Gurley number was normalized by the final film thickness (not shown here), it would be observed that there is a slightly higher normalized Gurley for a film cold stretched at 90 percent versus those stretched at either 65 or 80 percent. In fact, the local minima in normalized Gurley would occur at approximately 80 percent cold stretch. Upon further analysis of the data within Fig. 4.20, it is discovered that the temperature of cold stretching also influences the Gurley number. Specifically, the Gurley number decreases when comparing an A1-T_{cs}40 stretched film to an equivalent A1-T_{cs}70 stretched film. However, upon increasing the cold stretch temperature to 90°C, the Gurley number decreases. In fact, films produced using a cold stretch temperature of 90°C possess the lowest permeability (largest Gurley) versus other films presented in that figure with similar %CS values. The morphology of the A1 stretched film A1-T_{cs}90, as obtained via AFM, is displayed in Fig. 4.21. For comparison purposes, the reader will recall Fig. 4.20a – the AFM micrograph of a membrane produced with the standard condition. In comparing these two films, it is evident that the final film A1-T_{cs}90 possesses a lower micropore concentration at the surface than does that displayed in Fig. 4.20a. T his finding aids in explaining the higher Gurley numbers (lower porosity) that occurred for films cold stretched at 90°C versus the films that utilized lower cold stretch temperatures. As an aside, the frequency of films breaking during stretching was higher as the cold stretch temperature decreased which is likely a consequence of a lack of amorphous mobility as the this stretching temperature was decreased.

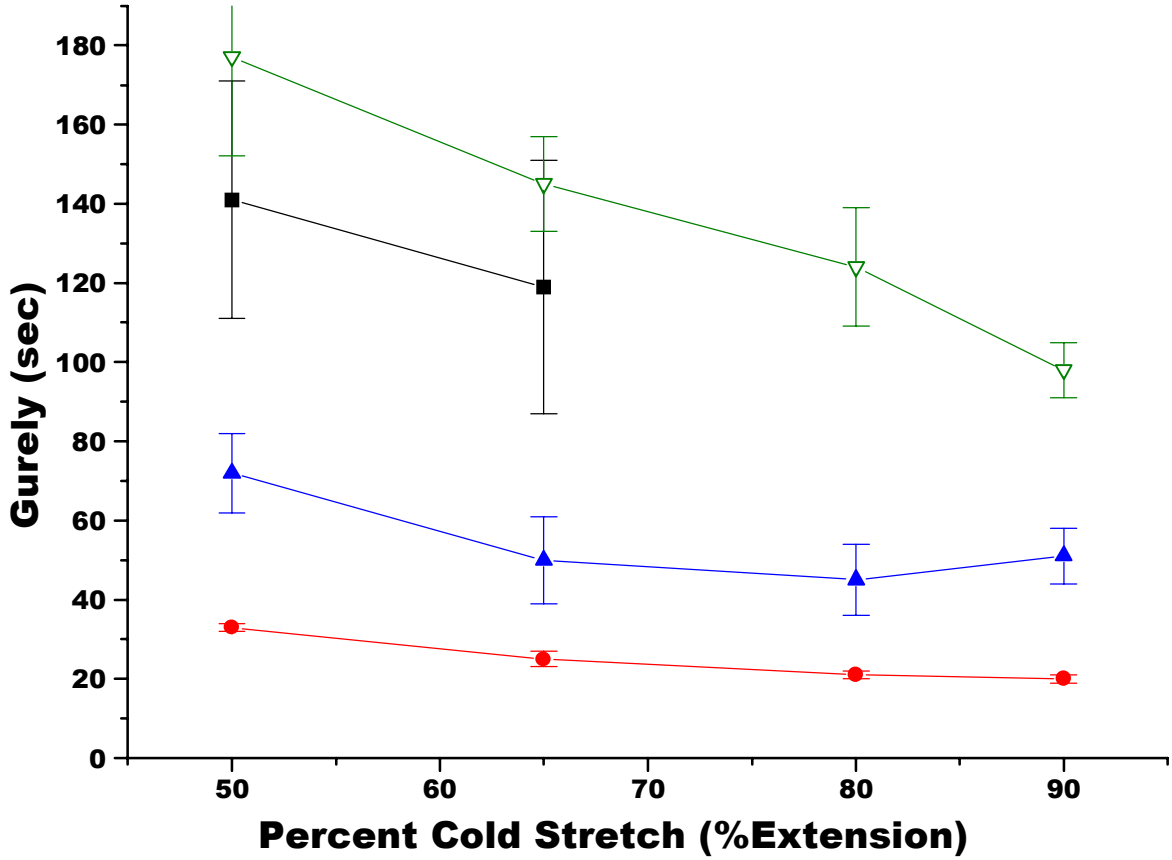

Figure 4.20 Effect of the cold stretch parameters (T_{cs} and %CS) on the Gurley number for A1 stretched films (-■-) T_{ca} = 40°C, (-●-) T_{ca} = 70°C, (-▲-) T_{ca} = 80°C, and (-▽-) T_{ca} = 90°C. The other annealing/stretching parameters remained constant with the standard condition.

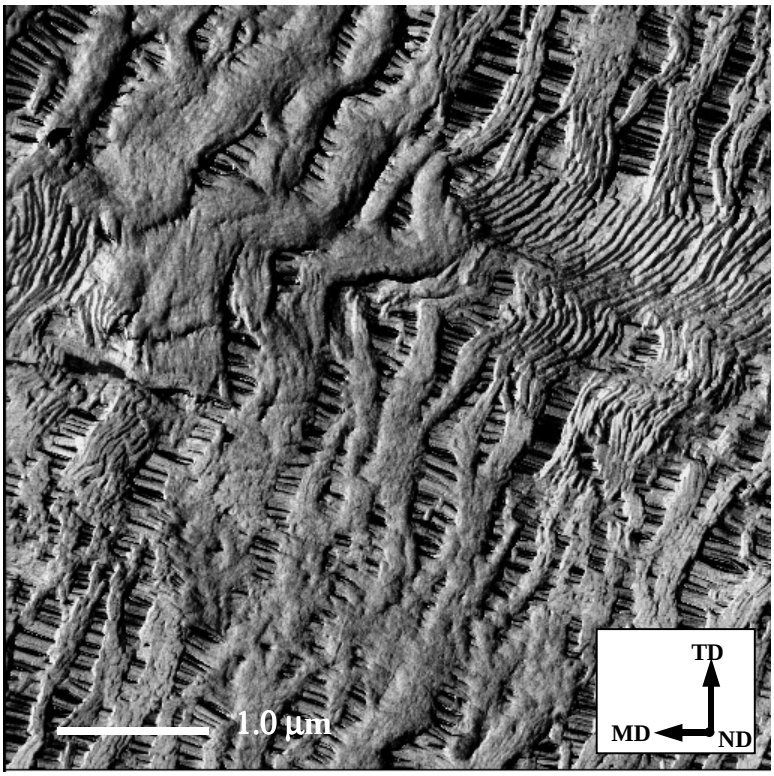

Figure 4.21 AFM phase image for the stretched membrane A1-T_{cs}90C. The MD is labeled. Image is 5µm x 5µm.

Gurley differences between A1 films of different cold stretch extension levels occurred because the cold stretch step acts to "nucleate" the micropores, where as the hot stretch step is utilized to increase or enlarge these structures. Thus, the more pore "nucleation" that transpires as a result of higher cold stretch levels, the more uniform and numerous the micropores will be in the final film. Figure 4.22 displays an AFM micrograph of a microporous film, where the film was produced employing the standard annealing/stretching conditions but *without* the standard hot stretch step. When it is compared with the film represented in Fig. 4.18d, the above statement is essentially verified. The reader may recall that the final film presented in Fig. 4.18d was produced utilizing the *entire* standard annealing/stretching condition.

Figure 4.23 is a plot indicating the dependence of the Gurley number on both the hot stretch step parameters (T_{hs} and %HS). Based upon the AFM micrograph in Fig. 22, which illustrated the effect of the hot stretch condition on the morphology, it was expected that the Gurley number for these films should decrease with increasing hot stretch extension. Indeed, as depicted in Fig. 23, the Gurley number decreased as the specific extension level is increased. However, if the Gurley numbers were normalized on membrane thickness, the film produced using the highest level of hot stretch extension (90%) possesses an equal if not a slightly higher normalized value versus the A1-%HS80 film. It is also observed in Fig. 4.23 that the hot stretch temperature, T_{hs}, influences the Gurley number. For a constant hot stretch level, the Gurley number decreased as the specific hot stretch temperature increased. This occurs regardless whether or not normalization of the Gurley number to film thickness was undertaken because for a constant total extension (i.e., %TS where %TS = %CS + %HS) the final film thickness was approximately the same.

If the effect of total percent stretch on the Gurley number was plotted, it would be similar to the behavior noted in either Figs. 4.20 or 4.23, because the reader only need to sum the percent cold stretch with percent hot stretch. In doing so, the total stretch values would be 100, 115, 130, and 140 percent extension for Fig. 4.23 and 140, 155, 170, and 180 percent for Fig. 4.20. The Gurley numbers corresponding to the stretched films with these %TS values are displayed in matrix form in Table 4.4 along with stretched films possessing other %CS and %HS combinations (the %TS is provided in the top left corner). All of the A1 stretched films displayed in this table possess Gurley numbers, which characterize these samples as being "quality" microporous membranes.

Table 4.4 The Gurley numbers and the %TS (top left corner of each cell) for A1 membranes. These membranes were products of different %CS and %HS combinations. All other annealing/stretching parameters remained intact with the standard condition.

%HS (%Extension) \ %CS (%Extension)	50	65	80	90
50	100% 48 ± 5	115% 35 ± 3	130% 34 ± 2	140% 30 ± 2
65	115% 36 ± 2	130% 30 ± 2	145% 28 ± 3	155% 24 ± 1
80	130% 36 ± 2	145% 27 ± 1	160% 23 ± 2	170% 19 ± 2
90	140% 33 ± 1	155% 25 ± 2	170% 21 ± 1	180% 20 ± 1

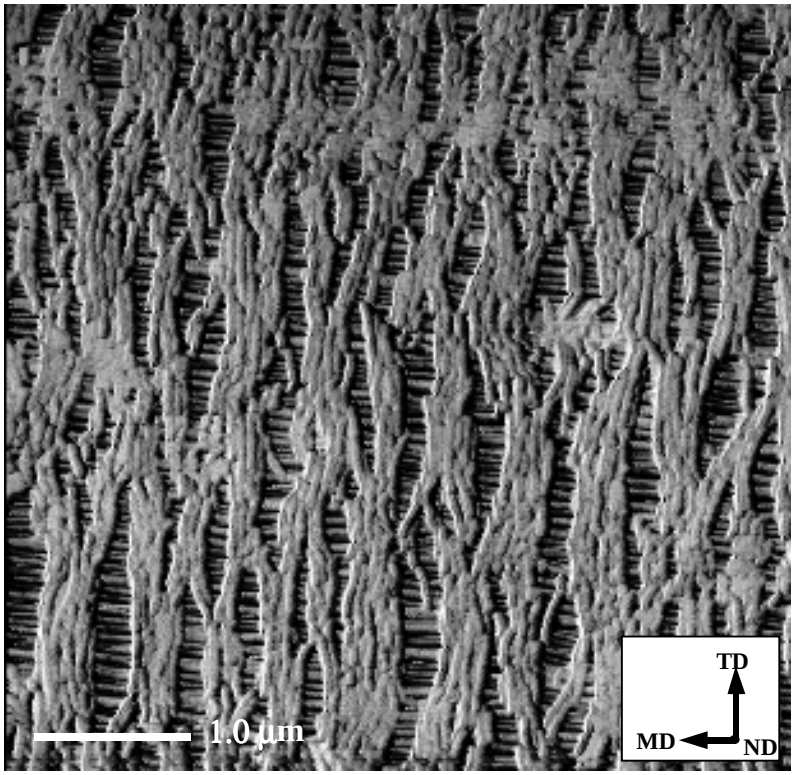

Figure 4.22 AFM phase image for an A1 stretched membrane where the standard hot stretch step was not used. The MD is labeled. Image is 5µm x 5µm.

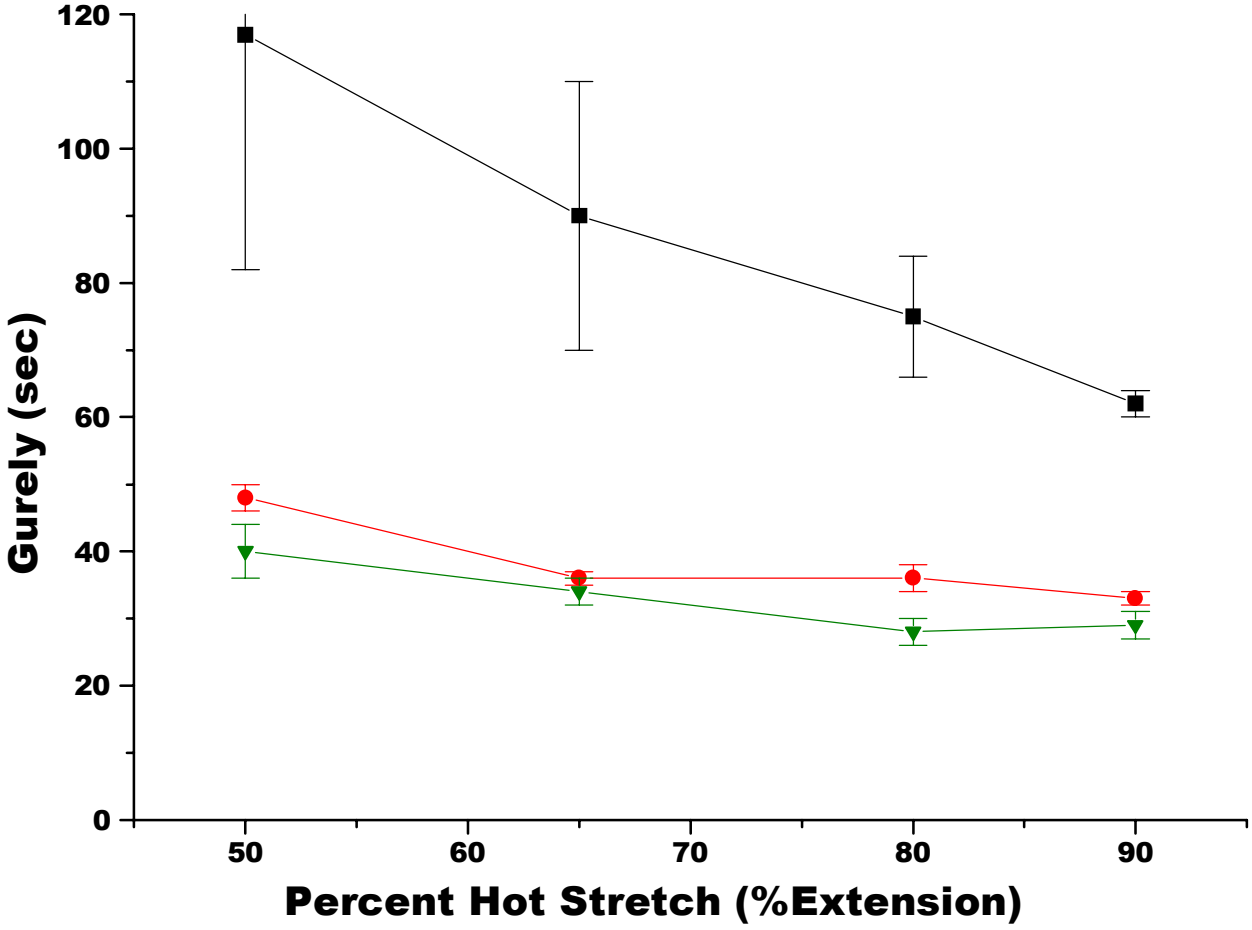

Figure 4.23 Effect of the hot stretch parameters (T_{hs} and %HS) on the Gurley number for A1 stretched films (-■-) T_{ca} = 120°C, (-●-) T_{ca} = 160°C, and (-▲-) T_{ca} = 180°C. The other annealing/stretching parameters remained constant with the standard condition.

It was also recognized that if the percent total stretch remains constant, there does not appear to be any *significant* benefit to final film permeability if the percent cold stretch is larger than the percent hot stretch within the total range of the stretching conditions studied. The effect of the total stretch on the final film morphology, as viewed with AFM, is shown for the two extreme cases of 100 and 180 percent in Figs. 4.24a & b, respectively. There is a slight observable difference in the micropore size between the 100 and 180 percent total stretch films, where the film produced using the larger total stretch is characterized by the larger micropore structure. Thus, the permeability difference between these films is accounted for. These results just presented are characteristics of membranes produced by annealing and stretching variable combinations, which did not utilize a relaxation step, i.e. the relaxation utilized was zero percent. A relaxation step is, however, generally employed in the industrial process to allow the stretched films to partially recover (shrink) after finishing the hot stretch step. The effect of such a relaxation step on the micropore structure and film permeability has been ignored in this report until now. In Fig. 4.25, the Gurley number is displayed as a function of the percent relaxation (%rlx) for three A1 stretched films. One of these films, A1-%rlx0 has previously been presented as the stretched film utilizing the standard condition. The other films, A1-%rlx20 and A1-%rlx40, that utilize 20 and 40 percent relaxation, respectively, clearly indicate that by increasing the amount the film is allowed to relax, the Gurley number increases. In fact, the stretched sample allowed to relax the most, A1-%rlx40, possesses a Gurley number of ca. 150 seconds thereby indicating the lack of a “quality” microporous membrane. Within error, a non-quality Gurley number also characterizes the A1 membrane produced with 20 percent relaxation, A1-% rlx20.

In a similar manner to the resin A films, resin B and C films, B1 and C1, were annealed and subsequently stretched utilizing a number of the same variable combinations discussed. However, the results were dramatically different as are shown in Fig. 4.26a & b, respectively. In Fig. 4.26a, a typical AFM micrograph for a B1 final film is displayed. This film was produced with the standard annealing/stretching condition. It is clearly evident that this sample is absent of any microporous structure, and analogous results were observed for *all* other annealing and stretching variable combinations utilizing resin B precursors. Figure 4.26b also displays the lack of a microporous morphology. This AFM micrograph characterizes the stretched C1 film in which the standard stretching condition was also used. As with the resin B stretched films, the resin C films when stretched under an array of variable combinations were *all* devoid of a

microporous structure, thus, no further results concerning the films of resins B and C will be presented here.

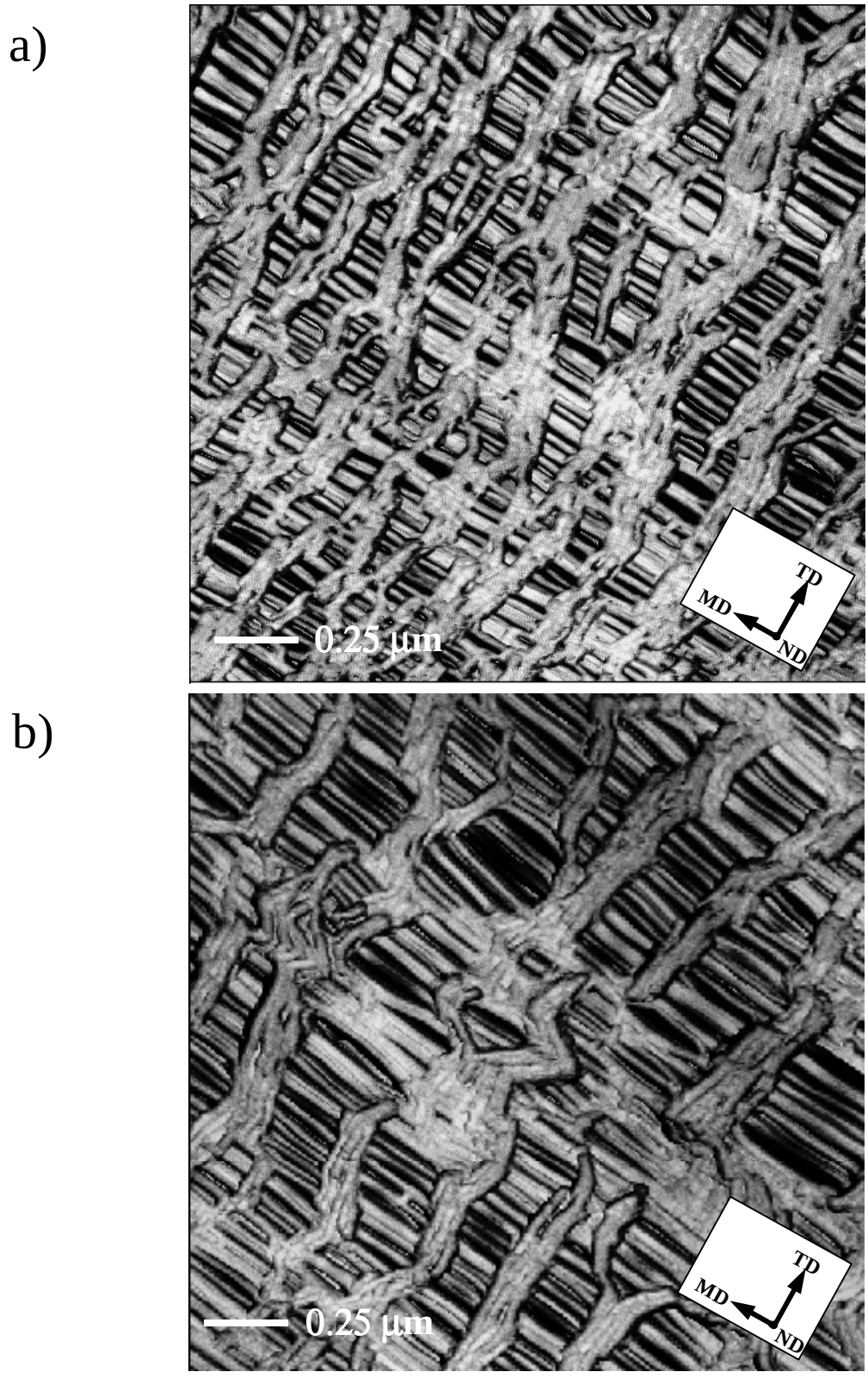

Figure 4.24 AFM phase images displaying the influence of total extension level (%TS) during stretching on A1 membrane morphology: a) %TS = 100% and b) %TS = 180%. The MD is labeled.

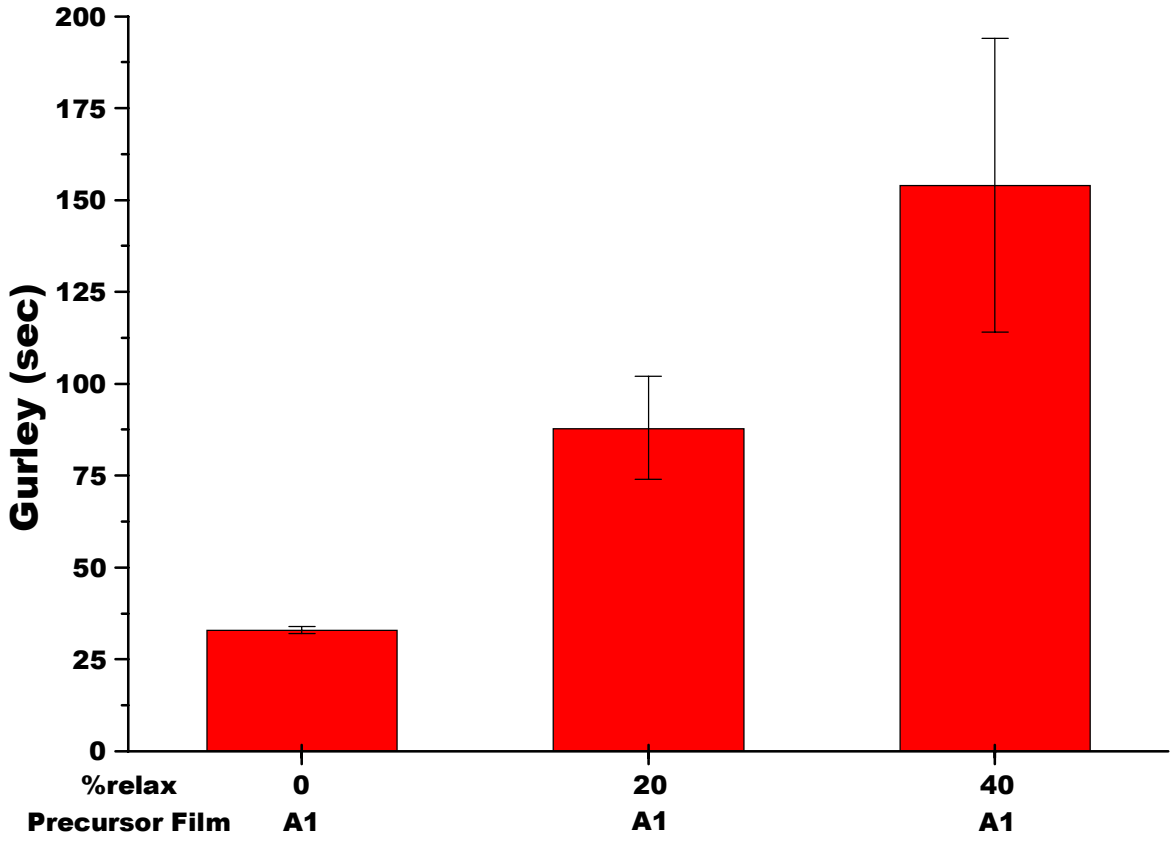

Figure 4.25 Effect of the percent the film is allowed to relax from the %TS after hot stretching on the Gurley number for A1 stretched films. The other annealing/stretching parameters remained constant with the standard condition.

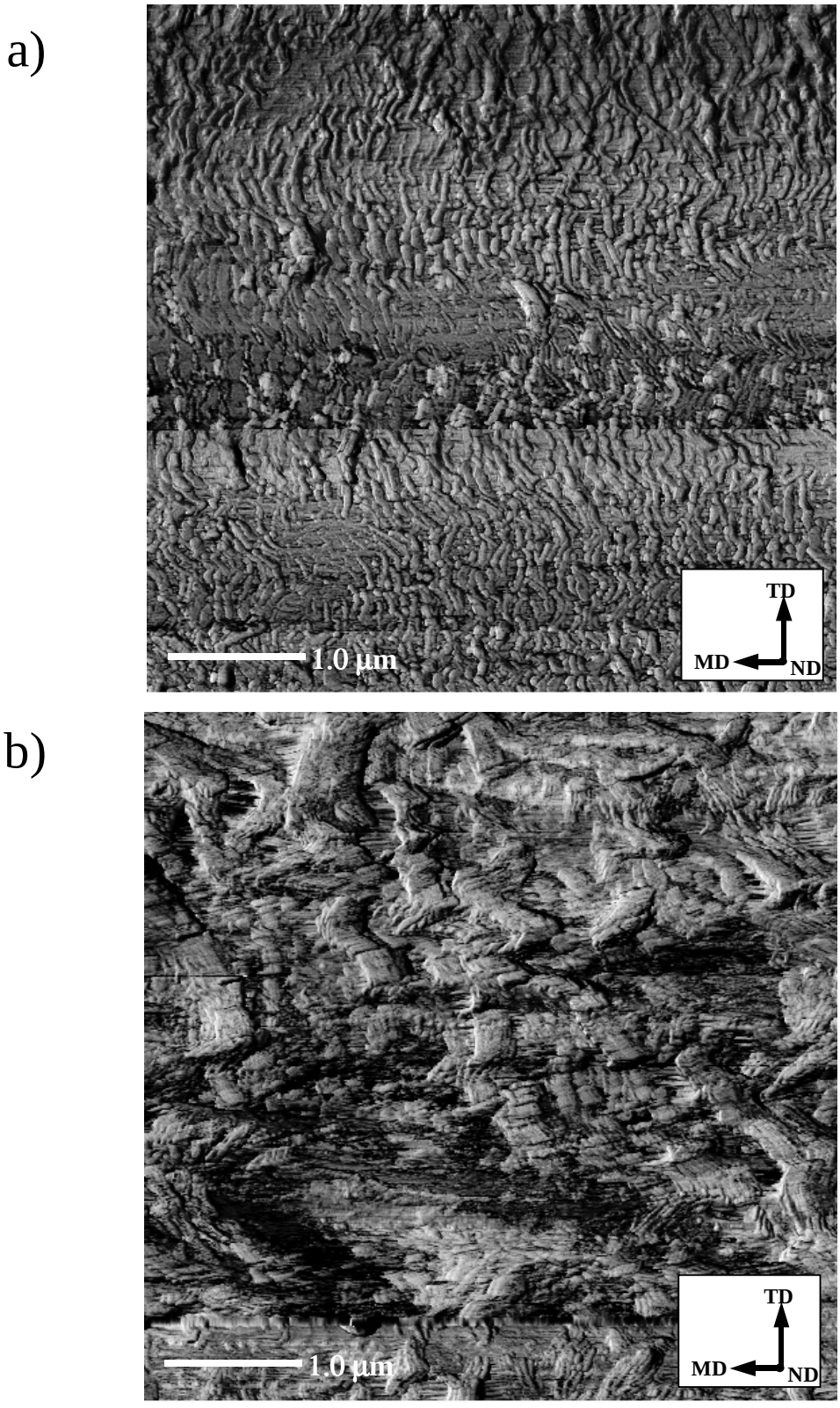

Figure 4.26 AFM phase images of the a) B1 and b) C1 stretched films produced utilizing the standard annealing/stretching conditions. The MD is labeled. Images are 5µm x 5µm.

4.4 DISCUSSION

The annealing results presented clearly indicated that the physical properties of the film including morphology, chain axis crystal orientation (f_c), melting point (T_m), and the degree of crystallinity (X_c) can be controlled to varying degrees by the annealing temperature (T_a), annealing time (t_a), and the level of extension or tension. When uniaxial tension was applied during annealing, the morphology that resulted was the product of lamellar separation. This produced interlamellar voids on the order of nanometers in size, as viewed by AFM on the sample surface. Optically, the films annealed at higher tension levels possessed visibly more haze than those annealed at lower tension levels. Regarding the TEM micrographs, the presence of micropores account for the increasing visible whitening or haze as the level of tension was increased. Similar TEM results have been observed by Zhou and Wilkes for HDPE films when tension (extension) was applied, where the initial films also possessed well-defined stacked lamellar morphologies.[28] It was further reported that the main chain orientation increased for the HDPE films with increasing deformation during annealing. In our PMP films, as the annealing tension level was increased, the crystalline orientation also increased as expected. However, this annealing parameter did not affect the percent crystallinity (X_c) or the melting point (T_m) of our samples.

In the case of increasing the annealing temperature or time utilized, the annealed film crystallinity correspondingly increased. The melting temperature, however, was less influenced by these two annealing variables. Thus, the annealing temperature and time spent in the PMP α_c relaxation are two factors that distinctly influence the resulting crystallinity. The α_c relaxation for a given semicrystalline polymer is attributed to main chain translational mobility within the crystalline phase and thus given a sufficient temperature to activate this relaxation, redistribution of the tight folds, loose loops, and lengthening of the tie chains can occur according to some researchers.[11,13,16] These effects, according to Rault[10], explain why annealing at elevated temperatures for longer times improves the rupture properties of semicrystalline materials that possess an α_c relaxation. Indeed, we reported that the frequency of film rupture decreased as the T_a or t_a utilized was increased, which was regardless of the stretching conditions.

The stretching conditions were shown to impact the final film properties such as the pore structure and permeability. The total amount of stretch was one such variable that influenced these properties. Greater overall film extension produced larger micropores (as was observed via AFM in Fig. 4.24) thus resulting in membranes of lower Gurley number (higher permeability).

Of the final films presented, the membrane possessing the lowest Gurley number was attained utilizing the highest total stretch (180%).

We now discuss the influence of the cold stretch temperature on the Gurley number and pore size. As shown in the results presented, this variable was found to influence film permeability in that as this stretching temperature increased from 40 to 70°C, the Gurley decreased. However, upon increasing the temperature above 70°C, the Gurley number increased. This result is also displayed below in Table 4.5 where the Gurley number dependence on various cold and hot stretch temperature combinations is presented. The initial decrease in Gurley number with increasing cold stretch temperature is a result of greater mobility within the amorphous phase rather than the crystal phase. This is because at 40°C a difference of only 5°C exists between the cold stretch temperature and the PMP glass transition of 35°C. The more limited amorphous mobility at 40°C also accounts for the greater frequency of film rupture during stretching relative to higher cold stretch temperatures. However, upon stretching at the higher cold stretch temperatures, the chain axes are able to translate through the crystal more readily as a result of greater activation of the α_c relaxation. The result is that at the lower cold stretch temperature of 70°C, the lamellae behave more solid-like (less chain-slippage through the lamellae), therefore, greater micropore nucleation is possible with the end result being more numerous micropores as was observable via AFM.

While chain slippage in the crystalline phase is not desirable for the cold stretching step, it is exactly the desired outcome in the hot stretching step. This results in greater lamellae separation as a consequence of higher levels of draw. As displayed in Table 4.5, one notes that the Gurley number is lowest for a hot stretch temperature of 180°C. At lower hot stretch temperatures, the Gurley values were not as low when compared with films hot stretched at 180°C, all other EUAS variables being equal.

Table 4.5 The effect of different T_{cs} and T_{hs} combinations on the resulting A1 microporous film Gurley number – all other annealing/stretching parameters remained constant with the standard condition.

T_{hs} (°C) \ T_{cs} (°C)	40	70	80	90
120	NP	62 ± 2 sec	88 ± 14 sec	NA
160	141 ± 30 sec	33 ± 1 sec	66 ± 10 sec	177 ± 25 sec
180	86 ± 16 sec	29 ± 2 sec	34 ± 4 sec	67 ± 12 sec

*NP denotes a sample that was not able to be produced because sample rupture occurred repeatedly for a number of attempts during cold stretching.
**NA denotes a variable combination that was not attempted.

From the above results, the porosity dependence on the annealing and stretching parameters was obtained. For the conditions analyzed, the highest membrane permeability for the resin A films was achieved utilizing an annealing temperature of 205°C for 20 min. without tension (free-annealed) followed by cold stretching the film at 70°C and hot stretching at 180°C. Previously, however, the dependence of the cold stretch extension level was based on a hot stretch temperature of 160°C instead of 180°C – recall Fig. 4.20. In Fig. 4.27, the Gurley number as a function of percent cold stretch is displayed where the data presented in this figure are based on a hot stretch temperature of 180°C. As expected, the absolute lowest Gurley number of 16 seconds occurs for the sample possessing the highest total stretch (180%). Upon normalization of the Gurley numbers to final film thickness, as displayed in Table 4.6, it is noted that the lowest normalized value was achieved with a percent cold stretch of 80 percent and thus a total stretch of 170 percent. Therefore, for the resin A films, the optimum annealing/stretching condition utilizes a film that is free-annealed at 205°C for 20 minutes followed by cold stretching at 70°C to 80 percent extension and then hot stretching at 180°C to 90 percent. This, however, is without the implementation of a relaxation step after the hot stretching step as it was found that the relaxation step decreases pore size and thus film permeability.

Table 4.6 Final A1 film Gurley numbers, film thickness, and normalized Gurley numbers as a function of the %CS – all other annealing/stretching parameters remained constant with the standard condition.

Sample	A1-%CS50	A1-%CS65	A1-%CS80	A1-%CS90
Gurley No. (sec)	29 ± 2	22 ± 1	17 ± 1	16 ± 1
Film Thickness (mil)	0.64	0.60	0.58	0.54
Normalized Gurley No. (sec/mil)	45	37	29	30

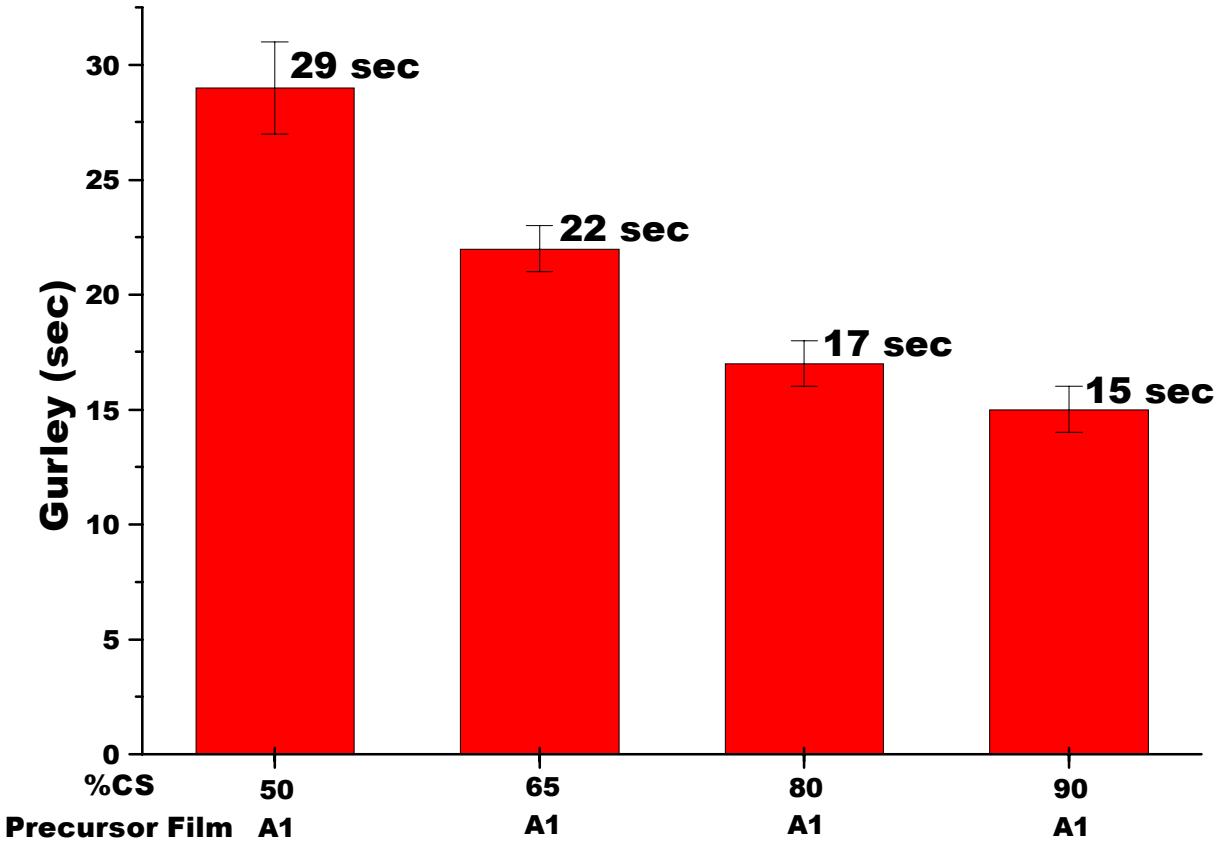

Figure 4.27 Gurley number dependence on cold stretch extension level (%CS) for A1 stretched films using T_{ha} = 180°C. The other annealing/stretching parameters remained constant with the standard condition.

The effect precursor f_c and morphology have on the stretched film permeability and structure has yet to be discussed. It was discovered that the precursor A1, when annealed and stretched at similar conditions to the A2 sample, possessed a higher permeability. It is reiterated that precursor A1 was characterized by a slightly more planar lamellar morphology and a higher f_c value with respect to the MD than the precursor A2. Therefore, starting film morphology and orientation state have an integral role in the final film properties. In the vast majority of cases presented here, however, when annealed and stretched, resin A films were produced into microporous membranes.

The resin B or resin C films, however, did not form microporous morphologies when subjected to a large number of variable combinations identical to those applied to the resin A films. In the case of the resin B films, this result is attributed to its additional amount of comonomer that adversely impacted its α_c relaxation. In the case of the resin C films, it is the precursor properties, specifically morphology and f_c, that are believed to be the principal cause of poor microporosity. This conclusion regarding the resin C films is made since no other property with the exception of molecular weight was different from the resin A precursors. Additionally, the effect of f_c on permeability has already been shown to be of consequence in the case of the resin A films. Recall that the resin A final film comparison took place between precursors possessing f_c values of 0.89 and 0.83, which is a relatively small difference that resulted in a detectable difference in permeability. The resin C film C1 is thus significantly lower at 0.67 – note that this was the highest f_c value measured for any of the resin C precursors.

From the above results and discussion, it was evident that the annealing and stretching parameters studied here impacted the final film microporosity. Furthermore, it is suggested by the authors that the criteria or prerequisites a semicrystalline polymer must be able to fulfill in order to form a "quality" microporous membrane via the three stage MEAUS process are as follows:

1. "Fast" crystallization kinetics
2. A highly planar lamellae morphology for the extruded precursor
3. "High" orientation of the crystalline phase in the precursor
4. Proper film thickness (1mil) and quenching rate to facilitate rapid heat transfer of the film
5. Presence of a α_c relaxation

4.5 CONCLUSIONS

The annealing and uniaxial-stretching behavior of melt-extruded precursor films from three resins were studied where each film was characterized as possessing a stacked lamellar morphology. The end goal was to produce microporous films from these precursors by applying the appropriate conditions.

It was recognized that with increasing annealing temperature or annealing time, the crystallinity was increased while the melting point was not significantly affected. The morphology was observably affected only for annealing temperatures equal to or above 215°C applied for 20min. The application of tension during annealing also influenced the annealed film morphology. Lamellar separation was specifically found to occur by AFM and TEM. Further, a higher tension level during annealing produced an increase in crystalline orientation.

The initial melt-extruded morphology and crystal orientation were found to be influential on the microporosity and permeability of the final film. In fact, a lower orientation value and slightly twisted lamellar morphology was believed to be the main reason why the precursors from resin C were not able to form microporous membranes. Morphological alterations resulting from annealing with and without tension were also found to influence the microporosity. Annealing time and temperature were critical as well not only to the final film but also in minimizing the frequency of film rupture during stretching. Specifically, films annealed at lower temperatures for shorter times ruptured more often during stretching than films annealed at higher temperatures and longer times. This annealing effect on the film breakage for the PMP films was attributable to the presence of an α_c relaxation in the resin A films. This same relaxation was also used to account for other morphological effects that impacted the porosity. In the case of the resin B films, comonomer may have affected the α_c relaxation in such a manner that was detrimental to the formation of microporous films via the MEAUS process.

Acknowledgements

The authors would like to thank the Celgard Corporation LLC for their continuing financial assistance for this project as well as the informative discussions that have taken place with them. The authors also thank Stephen McCartney for aiding in TEM as well as AFM instruction.

References

[1] Cannon, S. L., McKenna, G. B., Statton, W. O., *Macromol. Rev.*, **11**, 209, (1976).
[2] Yu, T. H., Wilkes, G. L., *Polymer*, **37**, 4675, (1996); Erattum, **38**(6), 1503 (1997); *J. Rheology*, **40**(6), 1079 (1996).
[3] Yu, T. H., Ph.D. Dissertation (advisor: G. L. Wilkes) Virginia Tech, 1995.
[4] Kamo, J., Uchida, M., Hirai, T., Japanese Pat. 63[1988]-256712, 1988.
[5] Noether, H. D., U. S. Pat. 3,513,110 (May 19, 1970) Celanese Research Group.
[6] Gore, R. W., U. S. Pat. 39,621,253 (1967).
[7] Knobloch, R. W., Statton, W. O., U. S. Pat. 3,299,171 (Jan. 17, 1967) assigned to E. I. Dupont Denemours & Co., Inc.
[8] Johnson, M. B., Wilkes, G. L., submitted for publication to *JAPS*.
[9] Druin, M. L., Loft, J. T., Plovan, S. G., U. S. Patent 3,801,404, 1974, assigned to Celanese Corp.
[10] Rault, J., J.M.S.- Rev. Macromol. Chem. Phys., **C37**(2), 335, (1997).
[11] Popli, R., Mandelkern, L., Benson, R. S., *J. Polym. Sci., Polym. Phys. Ed.*, **5**, 407, (1984).
[12] Boyd, R. H., *Polymer*, **26**, 323, (1985).
[13] Boyd, R. H., *Polymer*, **26**, 1123, (1985).
[14] Marand, H., Xu, J., Srinivas, S., *Macromolecules*, **31**, 8219, (1998).
[15] Nakayasu, H., Markovitz, H., Plazek, D. J., *Trans. Soc. Rheol.*, **5**, 261, (1961).
[16] McCrum, N. G., Read, B. E., Williams, G., Anelastic and Dielectric Effects in Polymeric Solids, Wiley, New York, 1967.
[17] Zhou, H., Wilkes, G. L., *Macromolecules*, **30**, 2412, (1997).
[18] Celgard Corp. LLC, Product Literature.
[19] Aharoni, S. M., Sibilia, J. P., *Polym. Eng. Sci.*, **19**, 450, (1979).
[20] Porter, R. S., Wang, L., *J. Macromol. Sci., Rev. Macromol. Chem. Phys.*, **C35**(1), 63, (1995).
[21] Uehara, H., et al., *Polym. Journal*, 29, 198, (1997).
[22] Celgard Corp. LLC., Private Communication.
[23] Hermans, P. H., Hermans, J. J., Vermaas, D., Weidinger, A., *J. Polym. Sci.*, **3**, 1, (1947).
[24] He, T., Porter, R. S., *Polymer*, **28**, 946, (1987).
[25] Gabbay, S. M., Stivala, S. S., *Polymer*, **17**, 121, (1976).
[26] Choy, C. L., Luk, W. K., Chen, F. C., *Polymer*, **22**, 543, (1981).
[27] Lopez, L. C., Wilkes, G. L., Stricklen, P. M., White, S. A., *J. M. S. –Rev. Macromol. Chem. Phys.*, **C32**(3&4), 1992, 301.
[28] Zhou, H., Wilkes, G. L., *J. Mater. Sci.*, **33**, 287, (1998).